RESEARCH ARTICLE

Acquired Multidrug Resistance in AML Is Caused by Low Apoptotic Priming in Relapsed Myeloblasts

Elyse A. Olesinski[1,2], Karanpreet Singh Bhatia[3], Chuqi Wang[3], Marissa S. Pioso[1,2], Xiao Xian Lin[3], Ahmed M. Mamdouh[3], Shu Xuan Ng[3], Vedant Sandhu[3], Shaista Shabbir Jasdanwala[3], Binyam Yilma[1,2], Stephan Bohl[1,2], Jeremy A. Ryan[1,2], Disha Malani[1,2], Marlise R. Luskin[1], Olli Kallioniemi[4,5], Kimmo Porkka[6], Sophia Adamia[1], Wee Joo Chng[7], Motomi Osato[7], David M. Weinstock[1,2], Jacqueline S. Garcia[1], Anthony Letai[1,2], and Shruti Bhatt[3]

ABSTRACT

In many cancers, mortality is associated with the emergence of relapse with multidrug resistance (MDR). Thus far, the investigation of cancer relapse mechanisms has largely focused on acquired genetic mutations. Using acute myeloid leukemia (AML) patient-derived xenografts (PDX), we systematically elucidated a basis of MDR and identified drug sensitivity in relapsed AML. We derived pharmacologic sensitivity for 22 AML PDX models using dynamic BH3 profiling (DBP), together with genomics and transcriptomics. Using *in vivo* acquired resistant PDXs, we found that resistance to unrelated, narrowly targeted agents in distinct PDXs was accompanied by broad resistance to drugs with disparate mechanisms. Moreover, baseline mitochondrial apoptotic priming was consistently reduced regardless of the class of drug-inducing selection. By applying DBP, we identified drugs showing effective *in vivo* activity in resistant models. This study implies evasion of apoptosis drives drug resistance and demonstrates the feasibility of the DBP approach to identify active drugs for patients with relapsed AML.

SIGNIFICANCE: Acquired resistance to targeted therapy remains challenging in AML. We found that reduction in mitochondrial priming and common transcriptomic signatures was a conserved mechanism of acquired resistance across different drug classes *in vivo*. Drugs active *in vivo* can be identified even in the multidrug resistant state by DBP.

INTRODUCTION

Acute myeloid leukemia (AML) is characterized by the uncontrolled proliferation of undifferentiated myeloid progenitors. AML is an aggressive malignancy, where approximately two-thirds of patients undergo relapse after achievement of remission on standard-of-care cytotoxic chemotherapy, 7 + 3 regimen (combination of cytarabine and daunorubicin). After nearly four decades of unprogressive treatment regimens, the therapeutic landscape of AML has been changing since 2017, due to clinical approval of >8 new targeted therapies (1–3). These new targeted therapies are directed toward specific genetic lesions or independent of genetic mutations, including FLT-3 inhibitors (midostaurin, gilteritinib, and quizartinib; refs. 4–6), BCL-2 antagonist (venetoclax; ref. 7), gemtuzumab ozogamicin (anti-CD33 monoclonal antibody–drug conjugate; ref. 8), IDH1/IDH2 inhibitors (ivosidenib and enasidenib; refs. 9, 10), a Hedgehog inhibitor (glasdegib; ref. 11), and menin inhibitor (revumenib; ref. 12). Although these targeted therapies have provided encouraging clinical opportunities, there are new emerging challenges, including overcoming the emergence of acquired resistance to new targeted therapies and identifying individualized therapies to overcome acquired resistance. Hence, understanding if acquired resistance in AML is specific to each targeted therapy or specific to the patient's tumor is increasingly important now.

It has been largely presumed that genetically distinct subclones within a tumor display differential responses to drugs and are believed to be the main source of acquired resistance. Thus, major efforts in oncology have been devoted to identifying genetic mutations and characterizing the underlying mechanism of mutant genes as the relapse causing mechanism. There is compelling evidence in solid tumors for genetic evolution; for example, *T790M* mutations in driving epidermal growth factor receptor (EGFR) inhibitor resistance (13), *MAPK* alternations in driving RAF therapy resistance, and *ALK* mutations in driving ALK inhibitor resistance (14, 15). In AML, targeted therapy with FLT-3 inhibitors showed the emergence of genetic mutations at relapses in some cases, such as the *F691L* gatekeeper mutation, *D835Y/V/F* mutations in tyrosine kinase domains, and *NRAS/IDH2* mutations in FLT-3-independent clones, whereas *TET2/IDH1* in FLT-3-mutant clones. Although the identification of relapse-associated genetic mutations has explained the basis of acquired resistance in a minority of cases, the treatment outcomes from targeting relapse-associated mutations have been far less promising for a larger patient population. This is due to heterogeneity in mutation types and frequency across patients. In addition to genetic mechanisms, drug resistance at the molecular level could emerge from nongenetic mechanisms, epigenetic modifications, and alternations in tumor microenvironments (16–19). Because the relative contribution of mutational and nonmutational mechanisms to drug resistance remains unclear, designing effective treatment strategies for relapse patients has remained increasingly challenging.

[1]Department of Medical Oncology, Dana-Farber Cancer Institute, Boston, Massachusetts. [2]Harvard Medical School, Boston, Massachusetts. [3]Department of Pharmacy, National University of Singapore, Singapore. [4]Institute for Molecular Medicine Finland FIMM, Hi-Life, University of Helsinki, Helsinki, Finland. [5]Science for Life Laboratory, Department of Oncology and Pathology, Karolinska Institute, Solna, Sweden. [6]Hematology Research Unit Helsinki, University of Helsinki and Helsinki University Hospital Comprehensive Cancer Center, Department of Hematology, HUS, Helsinki, Finland. [7]Cancer Science Institute of Singapore, National University of Singapore, Centre for Translational Medicine, Singapore.

E.A. Olesinski and K.S. Bhatia are the co–first authors of this article.

Corresponding Authors: Shruti Bhatt, National University of Singapore, Department of Pharmacy, Science Drive 3, Blk S7, 02-16, Singapore, 129788. E-mail: Shruti_bhatt@nus.edu.sg; and Anthony Letai, Dana-Farber Cancer Institute, 440 Brookline Avenue, M430, Boston, MA 02215. E-mail: Anthony_letai@dfci.harvard.edu.

Blood Cancer Discov 2024;5:1–22

doi: 10.1158/2643-3230.BCD-24-0001

Notably, a striking majority—more than 80% of cytotoxicity—caused by chemotherapy and targeted therapies initiate tumor cell death by ultimately activating the mitochondrial pathway of apoptosis (7, 20–25). We previously demonstrated compelling evidence that baseline mitochondrial priming (threshold to apoptosis) predicts clinical response to conventional chemotherapy across different cancers, including AML (26, 27). Unlike chemotherapy, targeted therapy drugs are directed to genes/proteins of interest and, hence, the emergence of relapse could be specific to the targeted pathway. Although we acknowledge the multidimensional nature of resistance emergence, we speculate the possible existence of shared mechanisms of resistance to diverse classes of targeted therapies. Decades of oncology practice have consistently revealed a common theme: tumor cells at relapse are often difficult to kill due to possible multidrug resistance (MDR). This observation implies the presence of previously unexplored, shared pathways driving the emergence of resistance, and we hypothesize that effective targeting of common mechanisms could hold the key to actionable treatment strategies for relapsed patients.

Here, we first systematically model multiresistant phenotypes and then identify the common mechanisms driving relapse to targeted therapies. We applied a dynamic BH3 profiling (DBP) strategy that measures rapid changes in drug-induced apoptotic signaling using 40 drugs on 22 AML patient-derived xenografts (PDX) models. By applying unsupervised clustering on apoptotic priming readouts, we show that PDXs from treatment-naïve patients showed greater apoptotic priming responses than PDXs from relapsed or refractory (R/R) patients, implying MDR phenotypes at relapse. Similarly, drug-sensitivity responses to >500 drugs in Beat AML and Helsinki patients also showed that *ex vivo* drug-sensitivity response score was higher in diagnosis compared with relapsed patients (n > 1,000 patients; refs. 28–30). We generated *in vivo* acquired resistant models, transcriptomics, and DBP profiles of myeloblast pre- and post-resistance to understand the mechanism of MDR. We demonstrate that acquired resistance to targeted therapies in AML is accompanied by a common mechanism of reduction in mitochondrial priming, along with drug-specific resistance mechanisms. Finally, by testing multiple DBP-based predictions *in vivo,* we show that DBP can identify therapeutic vulnerability even in multidrug-resistant AML models. Our findings confirm MDR phenotypes at relapse and the existence of common nongenetic mechanisms as a key determinant for drug resistance emergence.

RESULTS

AML PDXs Derived from Relapsed Patient Samples Display an MDR Phenotype

One of the most consistent findings across all cancers, including AML, and all treatment types in oncology, is that relapsed tumors are almost always broadly less sensitive to a wide variety of agents compared with treatment-naïve cancers. We utilized PDX models to test our hypothesis due to the tractability of studying different leukemia treatment effects in a single human sample, by harnessing an abundance of samples and the opportunity to expand the same tumor and test it with multiple agents *in vivo* (31, 32). We established PDX models by injecting 0.6 million (passage-1) AML primary cells into an NSG host (Fig. 1A). Clinical characteristics of patients and their tumors from which PDXs were derived are indicated in Fig. 1B (32). We carried out next-generation sequencing (NGS) on 22 PDX tumors and matched normal specimens to identify somatic mutations and copy-number alterations (Fig. 1B; Supplementary Table S1). We exposed splenic myeloblasts isolated from PDXs (n = 22 models) with confirmed engraftment (>70% circulating hCD45$^+$ cells) to a drug panel for 14 hours. The drug panel included well-known receptor tyrosine kinase inhibitors, including FLT-3 receptor, EGFR, PI3K/AKT/mTOR (PAM pathway) inhibitors, epigenetic modulators, BH3 mimetics, and SMAC mimetics. We measured the drug-induced mitochondrial apoptotic priming response by measuring mitochondrial sensitivity to the promiscuously interacting BIM BH3 peptide, because BIM interacts with all antiapoptotic molecules and can directly activate BAX and BAK (33). As expected, there was a dispersion of drug sensitivity signals across the panels of drugs and PDX models. Of note, we found no specific correlation between PDX treatment status and genetic makeup.

In the clinic, a nearly universal finding is that patients with relapsed AML are less sensitive to most agents compared with treatment-naïve patients. To test if our DBP experiments mirrored clinical experience, we performed unsupervised hierarchical clustering of *ex vivo* DBP measurements across all drugs and all PDX models established from *de novo* (n = 10), primary refractory or relapsed patients (R/R, n = 10), and healthy donors (n = 3). Due to the nature of PDX models, the number of myeloblasts collected between models varied, such that some models were not exposed to all 40 agents. We selected the 27 drugs tested in all PDX models for unsupervised hierarchical clustering analysis (Fig. 1C; Supplementary Fig. S1A). We found that AML samples from treatment-naïve AML patients cluster together to the left where there is most chemosensitivity, whereas those obtained from patients with relapsed AML cluster together on the right, with few exceptions (cluster B1 vs. cluster B2, $P < 0.0001$). We find that the mean sensitivity pattern (delta priming score) of samples from treatment-naïve patients is distinct from that of the relapsed samples ($P < 0.0001$). Two treatment-naïve PDXs (DFAM-61786 and DFAM-68555) showed the highest delta priming response to most of the drugs on the panel. Cluster B1 contained all treatment-naïve PDXs (n = 7), except for 1 R/R PDX (Fig. 1C; Supplementary Fig. S1A). In contrast, cluster B2 was further divided into two subclusters of which B2.1 contained R/R PDXs (n = 6) that showed significantly lower priming than cluster A ($P < 0.0001$) and B1 ($P < 0.001$; Supplementary Fig. S1A). A subcluster B2.2 emerging from B2 had the lowest priming of all clusters, containing 3 R/R PDXs, 1 treatment-naïve PDX, and healthy monocytes/lymphocytes controls (cluster A vs. B2.2 $P < 0.0001$; cluster B1 vs. B2.2 ($P < 0.0001$); cluster B2.1 vs. B2.2 ($P < 0.05$); Supplementary Fig. S1A). Overall, we found that healthy CD34$^+$ cells were primed by less than 30% of drugs from the panel, reinforcing that most of these drugs are selectively priming myeloblasts and not CD34$^+$ cells (Supplementary Figs. S1A–S1C).

Unsupervised clustering of drugs also identified distinct patterns; the majority of targeted agents with an ability to induce priming only in a subset of PDXs were enriched within one

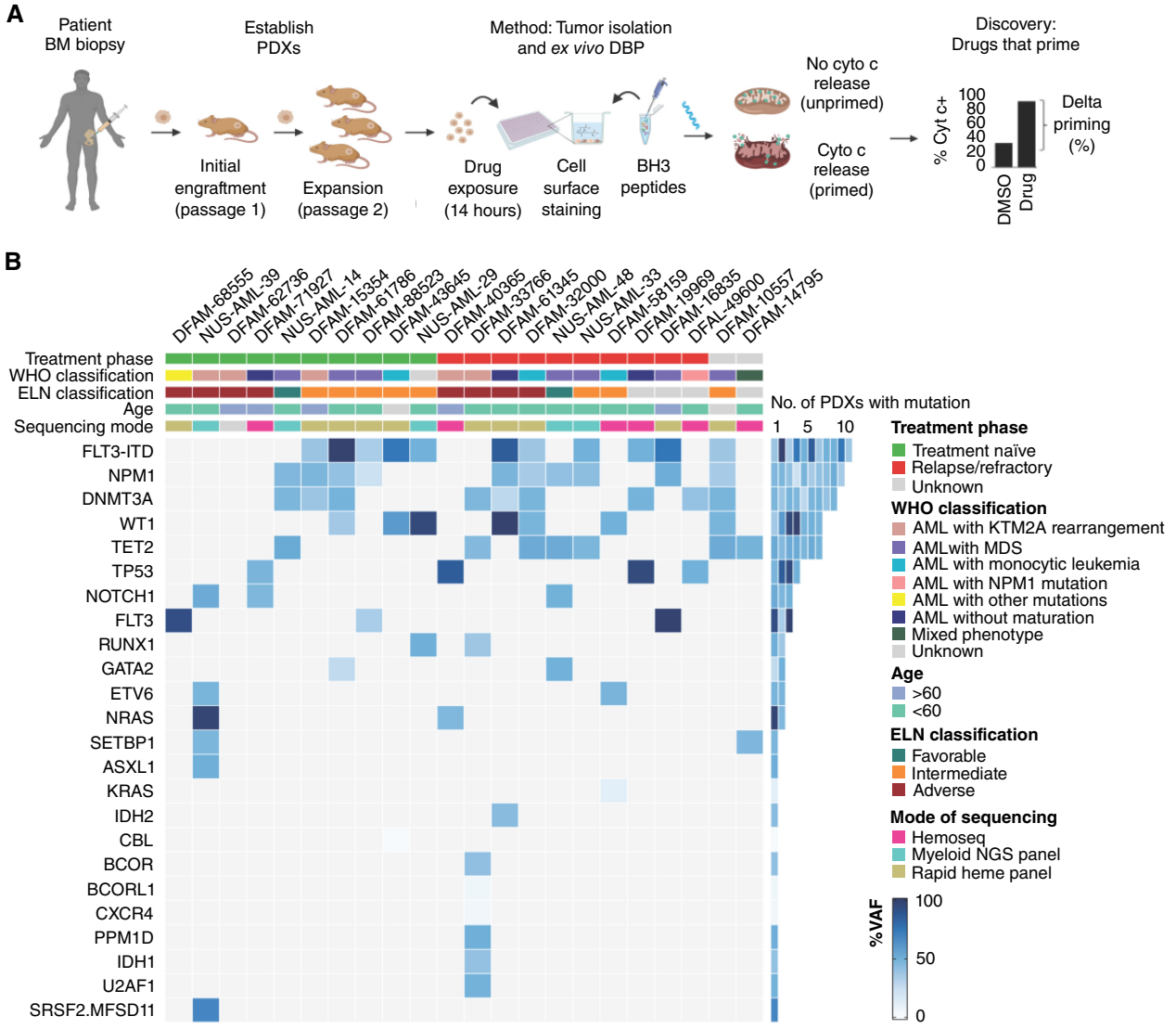

Figure 1. Drug-induced apoptotic priming classifies AML PDXs based on clinical outcomes. **A,** Schematic of generating PDX models and selecting drug candidates with DBP. BM, bone marrow. **B,** Clinical information of patients with AML at the point of bone marrow biopsy. Comutation heat map for genetic mutation present in the established PDX models (passage-2) determined by targeted exome sequencing for leukemia-related genes [rapid heme panel (RHP)] or Hemoseq or Myeloid NGS panel. WHO, World Health Organization; ELN, European LeukemiaNet; MDS, myelodysplastic syndrome; NGS, next-generation sequencing. (*continued on next page*)

cluster, including kinase inhibitors and epigenetic modifiers (Supplementary Fig. S1D). In contrast, a distinct subcluster of drugs showed sensitivity across a majority of PDXs, including BH3 mimetics, SMAC mimetics, CDK9 inhibitors, and HDAC inhibitors. We found that drugs with similar mechanisms of action clustered together (e.g., BRD-4 inhibitors OTXO-15, and JQ-1; CDK9 inhibitors AZD 4574 and AZD 4320). In summary, DBP results by themselves segregate samples in a way congruent with clinical context—clustering treatment-naïve, relapsed/refractory, and nonmalignant samples separately, in the order of broadly decreasing chemosensitivity.

We previously reported that baseline mitochondrial priming was able to predict the achievement of complete response and relapse to standard-of-care treatments in AML (7 + 3 combination; ref. 27). Having found that treatment-naïve PDX samples showed broadly greater sensitivity to many drugs compared with R/R samples, we asked whether they also had higher baseline mitochondrial apoptotic priming. Indeed, we observed that PDXs (without drug perturbation) established from R/R patients were less primed in response to both BIM ($P < 0.05$) and PUMA ($P < 0.01$) peptides than PDXs established from untreated tumors (Fig. 1D). Thus, it appears that relapsed myeloblasts have two distinct apoptotic signaling defects. They not only start with a lower level of mitochondrial priming but also the ability of drugs to increase apoptotic signaling appears blunted.

Generation of Drug-Resistant PDX Models

Having shown that PDXs established from R/R patients are multidrug resistant, we next sought to more broadly study mechanisms of MDR at relapse. To do this, we developed several models of *in vivo* acquired resistance (Fig. 2A).

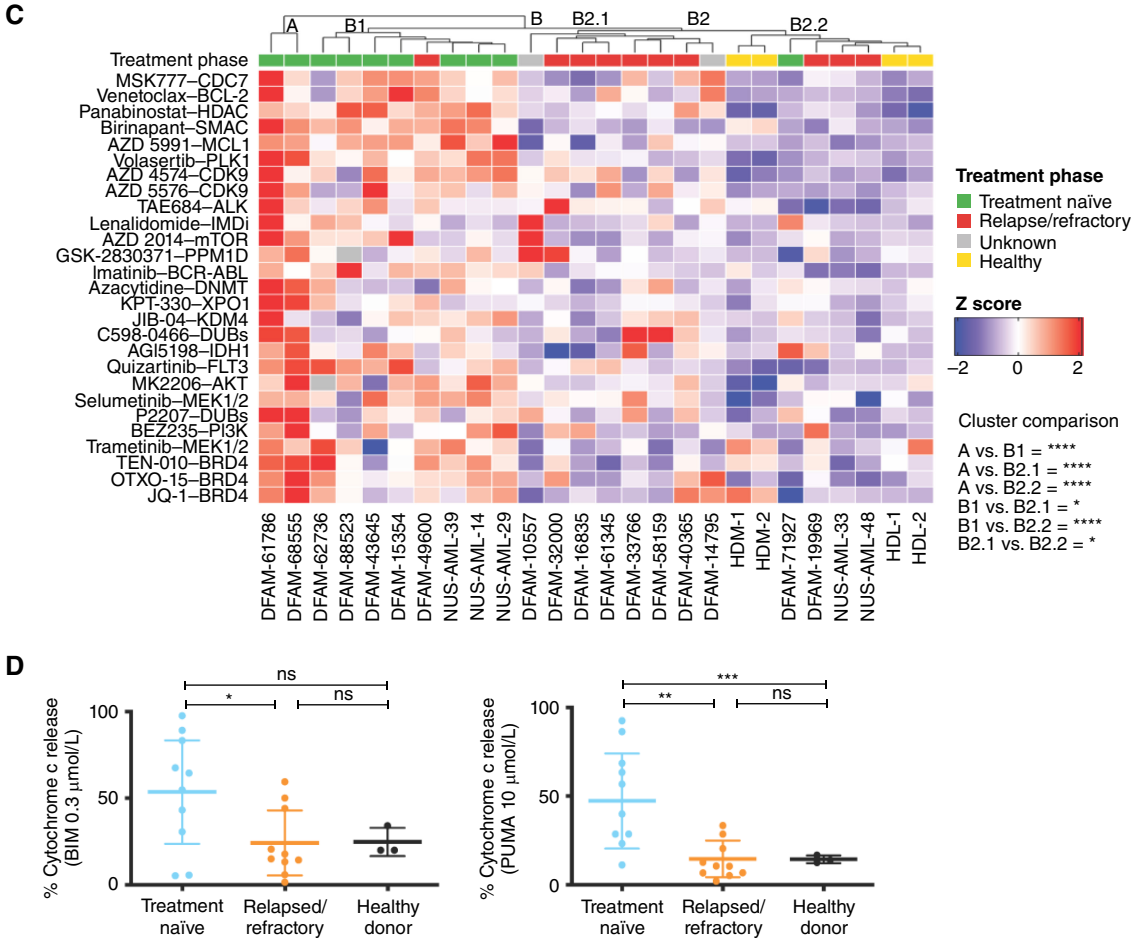

Figure 1. ***(Continued)*** **C,** Bone marrow mononuclear cells harvested from indicated PDX models ($n = 3$ mice/model) were exposed to targeted agents for 14 hours, followed by DBP to determine delta priming in response to BIM-BH3. Plotted here is unsupervised hierarchical clustering of delta priming values that are expressed in a heat map format. Delta priming = % cytochrome c release (drug-treated-DMSO treated cells). Each column indicates a mitochondrial sensitivity of AML PDXs and normal counterparts to indicated agents. Mean delta priming for cluster A (39.93%), cluster B1 (21.24%), cluster B2.1 (11.95%), and cluster B2.2 (3.84%) with comparisons via Welch *t* test. **D,** Baseline response of *de novo* and relapsed/refractory PDX models from **C** to BIM and PUMA BH3 peptides. Baseline profiles do not involve drug perturbation prior to exposure to the BH3 peptides. Horizontal line represents the median with interquartile range bars, one-tailed Mann–Whitney-rank sum test. *, $P < 0.05$; **, $P < 0.01$; ***, $P < 0.001$; ****, $P < 0.0001$; ns, no significance.

For resistance modeling, we selected drugs that showed high *in vivo* efficacy (<5% circulating peripheral blood blasts at day 15 of treatment) to specifically model acquired resistance. Drugs were prioritized based on their clinical relevance and pharmacokinetics. Four different PDX models (DFAM-61786, DFAM-15354, DFAM-61345, and DFAM-43645) of leukemia-bearing NSG mice were treated with quizartinib, birinapant, LCL-161, JQ-1, venetoclax, and S63845 until resistance emerged (Fig. 2B–F; refs. 20, 34). Although the time to relapse was highly variable, we successfully generated resistant models for all agents (Fig. 2B–F).

Distinct RNA Sequencing Signatures Define Drug-Resistant Phenotypes in AML PDXs

To investigate whether there were transcriptional signatures associated with acquired drug resistance, we used unbiased whole transcriptomic analysis on a total of 78 resistant samples from three PDX models (DFAM-61786, DFAM-15354, and DFAM-61345) and 16 matched-control samples (Fig. 3A; Supplementary Table S2). A total of 21,182 genes ranked by $\log_2$-fold change were identified from edgeR differential expression (DE) analysis, where most DEGs were upregulated in resistant samples compared with parent controls (Supplementary Fig. S2A and S2B). To determine biological pathways predictive of resistance, we performed gene set enrichment analysis (GSEA) on the list of ranked genes using a *P* value cutoff of 0.05, followed by KEGG pathway analysis.

Using those PDX models that acquired resistance to four distinct drugs, we first asked if there is evidence for the emergence of a common mechanism of resistance shared by different classes of targeted therapies. We identified a positive enrichment of pathways that included cytokine–cytokine receptor interactions, xenobiotics biodegradation, metabolic pathways, Hippo signaling, and Ras signaling (Fig. 3B; Supplementary Fig. S2C). Conversely, mechanisms relating to DNA repair and replication, such as base excision repair, mismatch repair, and homologous recombination, were negatively enriched (Fig. 3B; Supplementary Fig. S2C). We

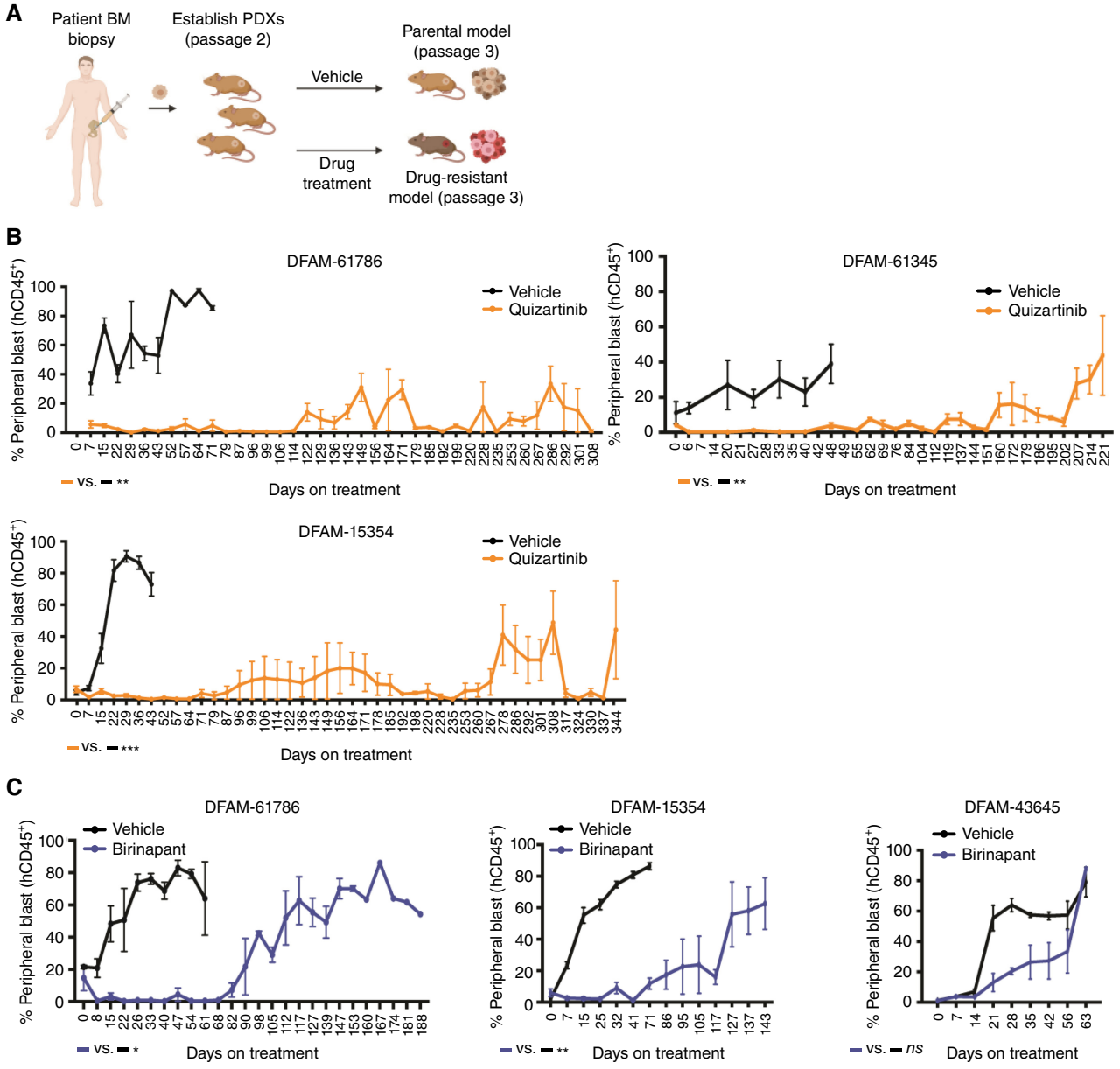

Figure 2. Modeling *in vivo* resistance to targeted therapy in AML. **A,** Schematic of *in vivo* drug resistance modeling. BM, bone marrow. *In vivo* disease progression over time in PDX models treated continuously with FLT-3 inhibitor quizartinib (**B**), SMAC mimetic birinapant (**C**), (*continued on next page*)

next focused on the emergence of pathway dysregulation in a drug-specific manner in the setting of acquired resistance. In quizartinib-resistant PDX models, we found significant enrichment (FDR < 0.05) in various prosurvival pathways, including Ras, JAK–STAT, PI3K–AKT, MAPK, TNF, FoxO, and Rap1 (Fig. 3C; Supplementary Fig. S2D and S2E). Birinapant-resistant PDX models showed downregulation in protein export mechanisms, mismatch repair, autophagy, and TCA cycle (Fig. 3C; Supplementary Fig. S2D). Venetoclax-resistant PDX models showed enrichment in numerous cell signaling pathways, including B cell, FoxO, and p53 downregulation in drug metabolism and protein export mechanisms (Fig. 3C; Supplementary Fig. S2D). Lastly, JQ-1-resistant PDX models revealed significant enrichment, specifically in spliceosome mechanisms and cAMP signaling pathways (Fig. 3C).

Having performed the combined analysis for samples derived from bone marrow and spleens of three PDX models, we next asked if there was a tissue-specific difference in the transcriptomic signatures for resistance emergence. Although we found pathways that are uniquely dysregulated in either bone marrow or spleen, we also saw common signatures. For instance, cAMP signaling, JAK–STAT signaling, and drug metabolism by cytochrome P450 were found to be enriched in bone marrow alone for all drug-resistant models (Supplementary Fig. S2C). In quizartinib- and

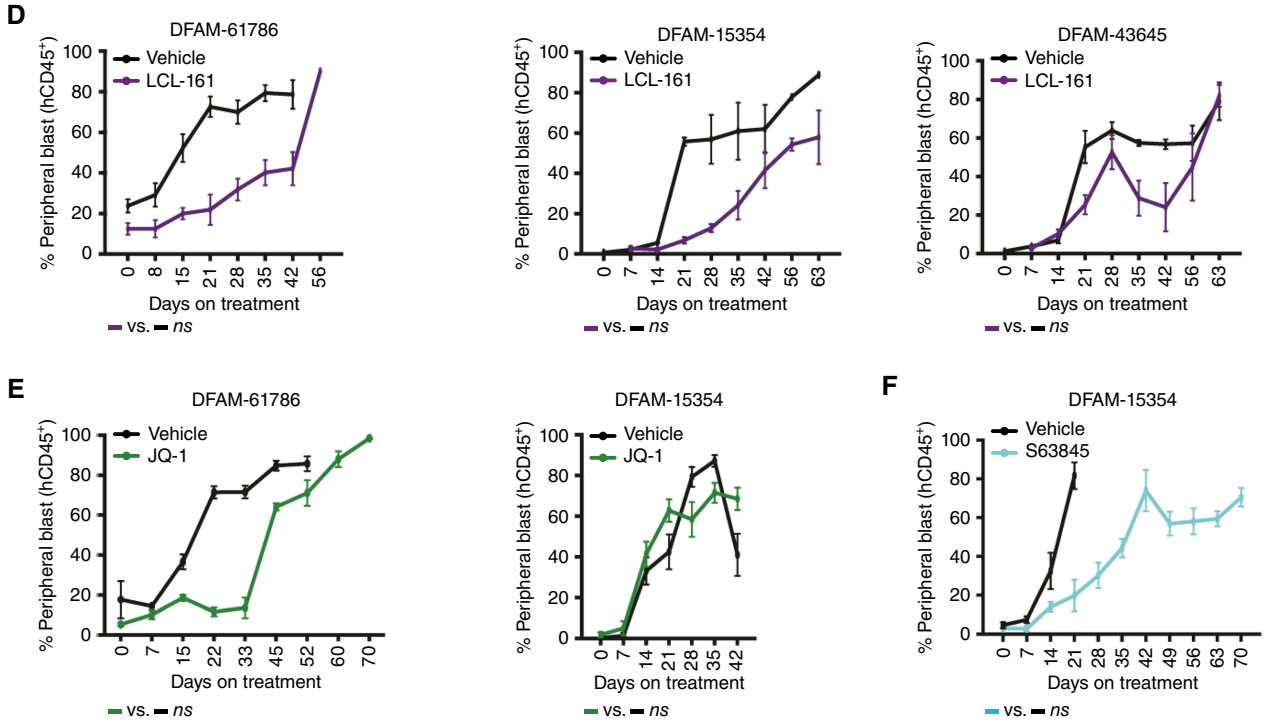

Figure 2. ***(Continued)*** SMAC mimetic LCL-161 (**D**), BRD-4 inhibitor JQ-1 (**E**), MCL-1 inhibitor S63845 (**F**), or vehicle, as measured by hCD45+ cells in the peripheral blood. PDX models were considered resistant once circulating hCD45+ cells reached >70% on treatment to indicated drugs. Error bars indicate mean ± SEM between 5 mice. For data on BCL-2 inhibitor venetoclax and MCL-1 inhibitor S63845 in DFAM-61786, please refer to (20). *, $P < 0.05$; **, $P < 0.01$; ***, $P < 0.001$; ns, no significance; vs, versus.

venetoclax-resistant models, greater enrichment or downregulation of gene-expression signatures was observed in spleen-derived myeloblasts compared with bone marrow, whereas the opposite was observed for birinapant-resistant models (Supplementary Fig. S2D). This suggests that tissue-specific gene signatures vary depending on the targeted therapy to which resistance was acquired.

To further validate the clinical relevance of resistance mechanisms observed in drug-resistant PDX models, we utilized an existing data set of AML patient transcriptomes (29). We compared RNA sequencing (RNA-seq) signature between relapsed ($n = 53$) and diagnosis ($n = 81$) samples from patients with AML (Fig. 3D; Supplementary Fig. S2B). Interestingly, we found overlap in gene-expression signatures enriched in drug-resistant PDX phenotypes and R/R patient samples (Fig. 3B and E; Supplementary Table S3). In both drug-resistant PDXs and relapsed primary AML, pathways associated with ECM–receptor interactions, cytokine–cytokine receptor interactions, JAK–STAT signaling pathways, calcium signaling pathways, ATP binding cassette (ABC) transporters, focal adhesion, Hippo signaling, RAS signaling, and PI3K–AKT signaling were upregulated, which are consistent with prior studies (Fig. 3B and E; Supplementary Table S3; refs. 35, 36).

One of the known MDR mechanisms to chemotherapy drugs in AML is increased expression of efflux pumps from the superfamily of ABC transporters (37). Hence, we next asked whether MDR mechanisms contribute to drug resistance to targeted agents in AML for some PDX models. We found enrichment in ABC transporter family pathway signatures in all three PDX models, DFAM-61786, DFAM-15354, and DFAM-61345, resistant to quizartinib, birinapant, and JQ-1 (Supplementary Fig. S3A). This was further supported by >4-fold increase in MDR pathway genes *ABCB11, ABCB4, ABCC8, ABCC9,* and *APOA1* in quizartinib- and birinapant-resistant PDX models (Supplementary Fig. S3B). Validation of RNA-seq findings using RT-qPCR showed a lower cycling threshold (CT) for *ABCB1* in DFAM-61786 and DFAM-61345, where parental controls showed no detectable *ABCB1* (Supplementary Fig. S3C). In addition, we validated enrichment for genes including *FGFR1, PARP1, MSH2*, which are essential for cell survival, migration, and DNA repair, respectively (Supplementary Fig. S3D, Supplementary Methods). We next asked whether observed enrichment in ABC transporter family genes in drug-resistant models resulted in higher drug efflux activity. To test this, we performed the calcein-AM efflux assay to assess p-glycoprotein (Pgp) activity in the birinapant-resistant and quizartinib-resistant DFAM-61786 PDX overexpressing *ABCB1*, which codes Pgp. We first validated the assay by showing time-dependent increase in FITC retention (Pgp substrate) after pretreatment with Pgp inhibitor, verapamil, in parental PDXs compared with DMSO controls (Fig. 3F; Supplementary Fig. S3E). As anticipated, birinapant-resistant and quizartinib-resistant cells treated with verapamil also displayed enhanced FITC retention compared with DMSO controls (Fig. 3F; Supplementary Fig. S3E).

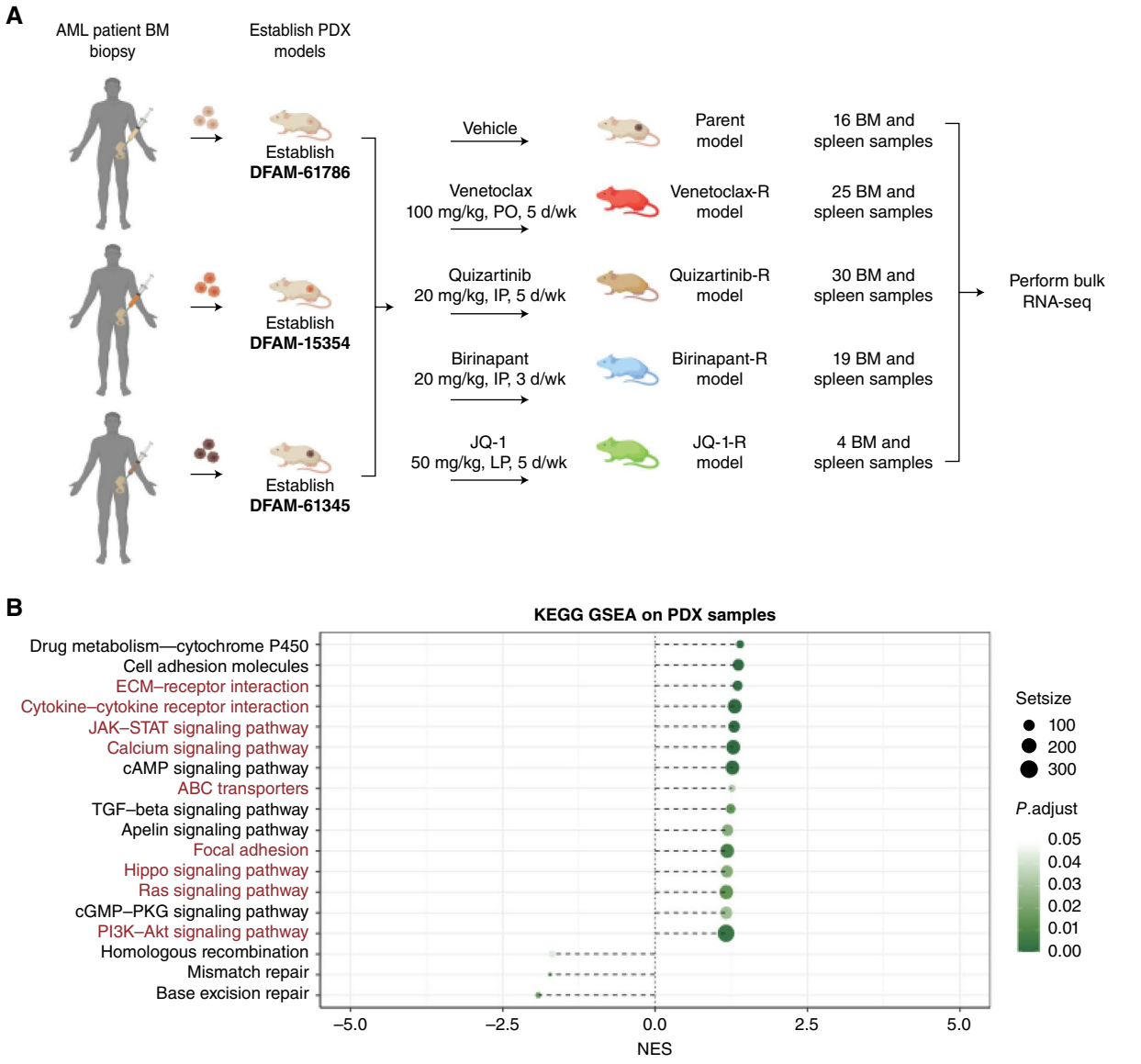

Figure 3. Transcriptome of resistant AML PDX models and primary tumors. **A,** Schematic for bulk RNA-seq performed on 78 resistant and 16 parent PDX model spleen samples from DFAM-61786, DFAM-15354, and DFAM-61345. **B,** Dot plot depicting GSEA on PDX samples using the KEGG database to identify differentially regulated pathways in all drug-resistant models compared with parental models. Red color indicates common differentially regulated pathways between the PDX samples and primary tumors in **E**. (*continued on next page*)

In Vivo Acquired Drug Resistance Selects for Reduction in Apoptotic Priming

After identifying drug-specific transcriptional signatures associated with acquired resistance, we next asked if the age-old, poorly explained phenomenon of acquired resistance to a single agent accompanied by MDR can be explained by a more general mechanism. Because many, if not most, targeted agents in AML kill via apoptosis, we wondered whether dampened apoptotic signaling might be an alternative mechanism underlying the *in vivo* acquisition of resistance to targeted therapies in AML that also leads to MDR. To test the hypothesis that the acquisition of drug resistance is accompanied by a global loss in mitochondrial priming, we performed baseline BH3 profiling on matched pre- and post-resistant PDXs (Fig. 4A). We designed the BH3 peptide panel to measure (i) overall apoptotic priming (BIM and PUMA); (ii) BCL-2 and BCL-XL dependence (BAD); (iii) MCL-1 dependence (MS-1); (iv) BCL-XL dependence (HRK); and (v) direct mitochondrial BH3 mimetic sensitivity (venetoclax and navitoclax; Fig. 4B). Across several different drugs with distinct mechanisms of action, acquisition of monotherapy drug resistance selected for decreased overall mitochondrial apoptotic priming, as demonstrated by relative insensitivity to the various BH3 peptides in drug-resistant PDXs compared with vehicle-treated PDXs (Fig. 4C; Supplementary Table S4). The exception was S63845, where resistance is not accompanied by substantial loss in overall priming (Fig. 4C). We previously showed that treatment with venetoclax led to leukemia

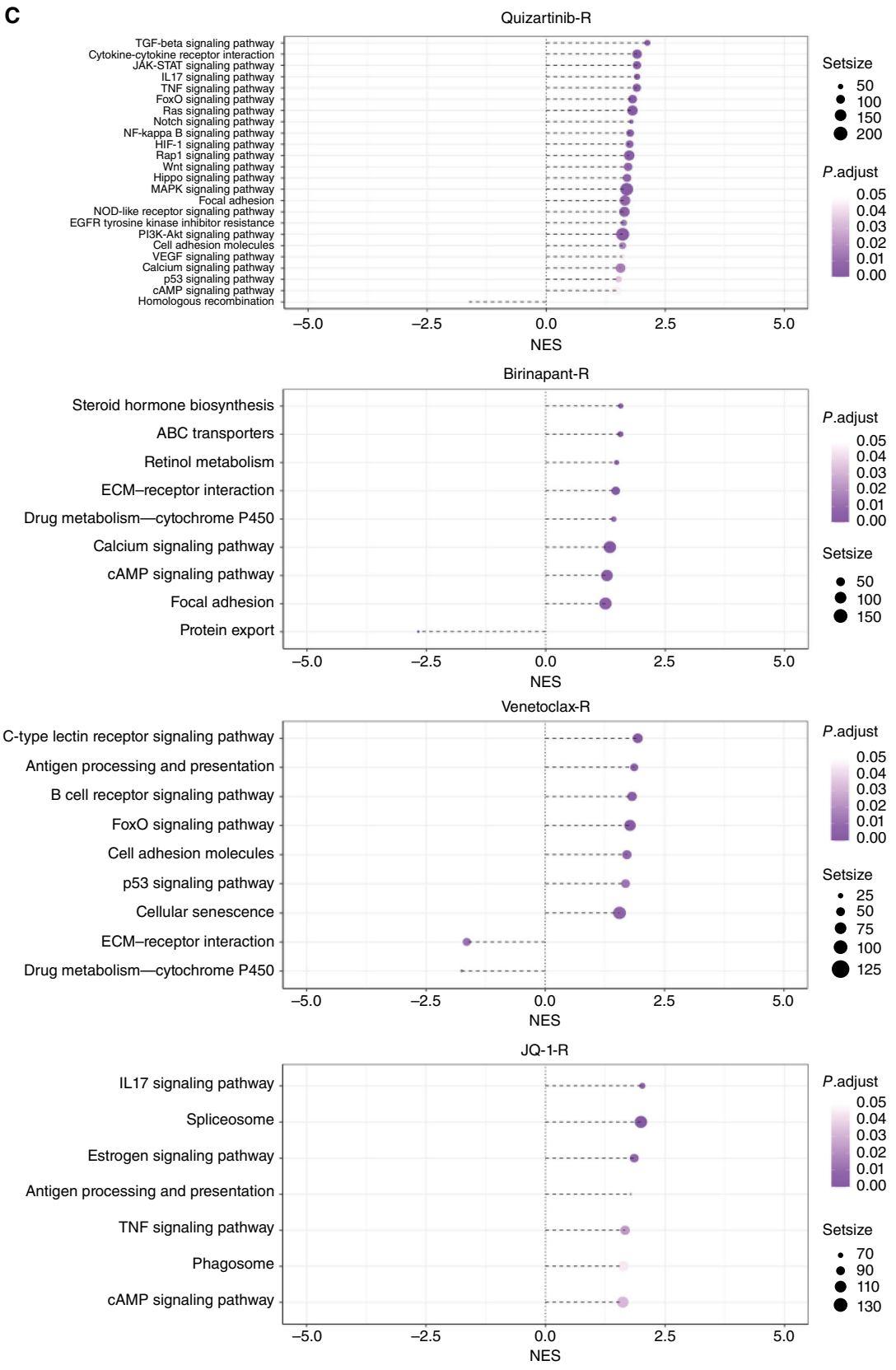

Figure 3. ***(Continued)*** **C,** Dot plot depicting GSEA results on PDX samples using the KEGG database for quizartinib-, birinapant-, and venetoclax-resistant PDX models compared with parental models. (*continued on following page*)

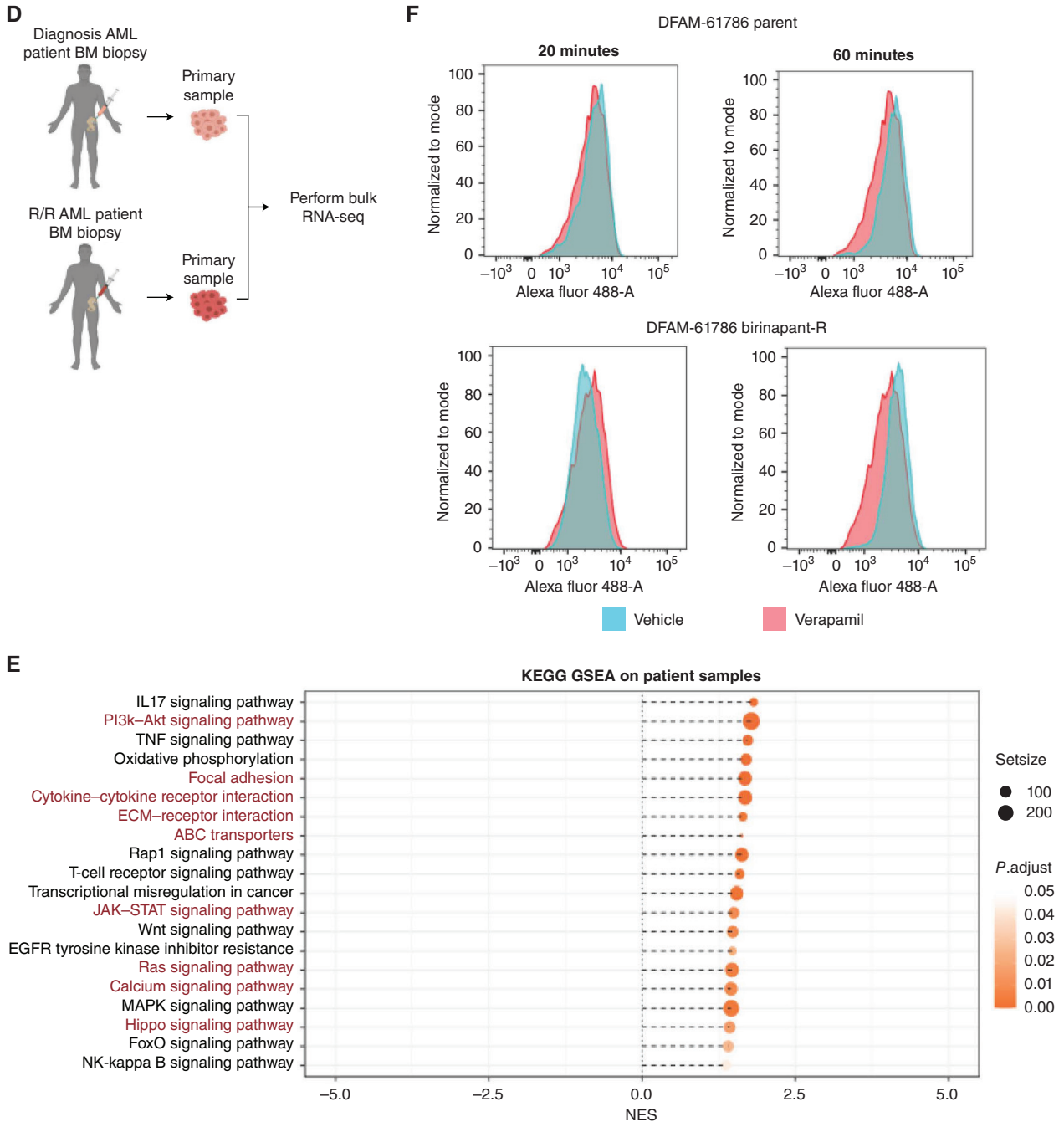

Figure 3. ***(Continued)*** **D,** Schematic for bulk RNA-seq on primary AML patient BM samples at diagnosis and relapse. **E,** Dot plot depicting GSEA on AML patient samples using the KEGG database. Red color indicates overlap in differentially regulated pathways between the AML primary tumors and PDX samples from **B**. **F,** Measurement of drug efflux activity using calcein-AM efflux in parental vs. birinapant-resistant PDX model DFAM-61786. Cells were treated for 10 minutes with verapamil followed by calcein-AM staining for 20 minutes. GSEA with adjusted $P < 0.05$ using Benjamini–Hochberg method. NES, normalized enrichment score. KEGG, Kyoto Encyclopedia of Genes and Genomes; ECM, extracellular matrix.

regression in S63845-resistant PDXs (20); therefore, we speculate that S63845 resistance is mainly mediated by expansion of BCL-2–dependent clones rather than apoptotically low/unprimed clones. Overall, these results suggest that though targeted agents affect a particular signaling pathway, during drug resistance, cells acquire loss of chemosensitivity not only via specific targeted mechanisms but also by selecting for globally reduced apoptotic signaling. The former might explain single drug-specific resistance, whereas the latter is a better explanation for the MDR that often arises in a relapsed tumor and how the phenomenon may act independent of the type of therapy and genetic background of the initial tumor.

Because we found PDXs that are treatment-naïve to be more primed compared with R/R PDXs (Figs. 1D and 4C),

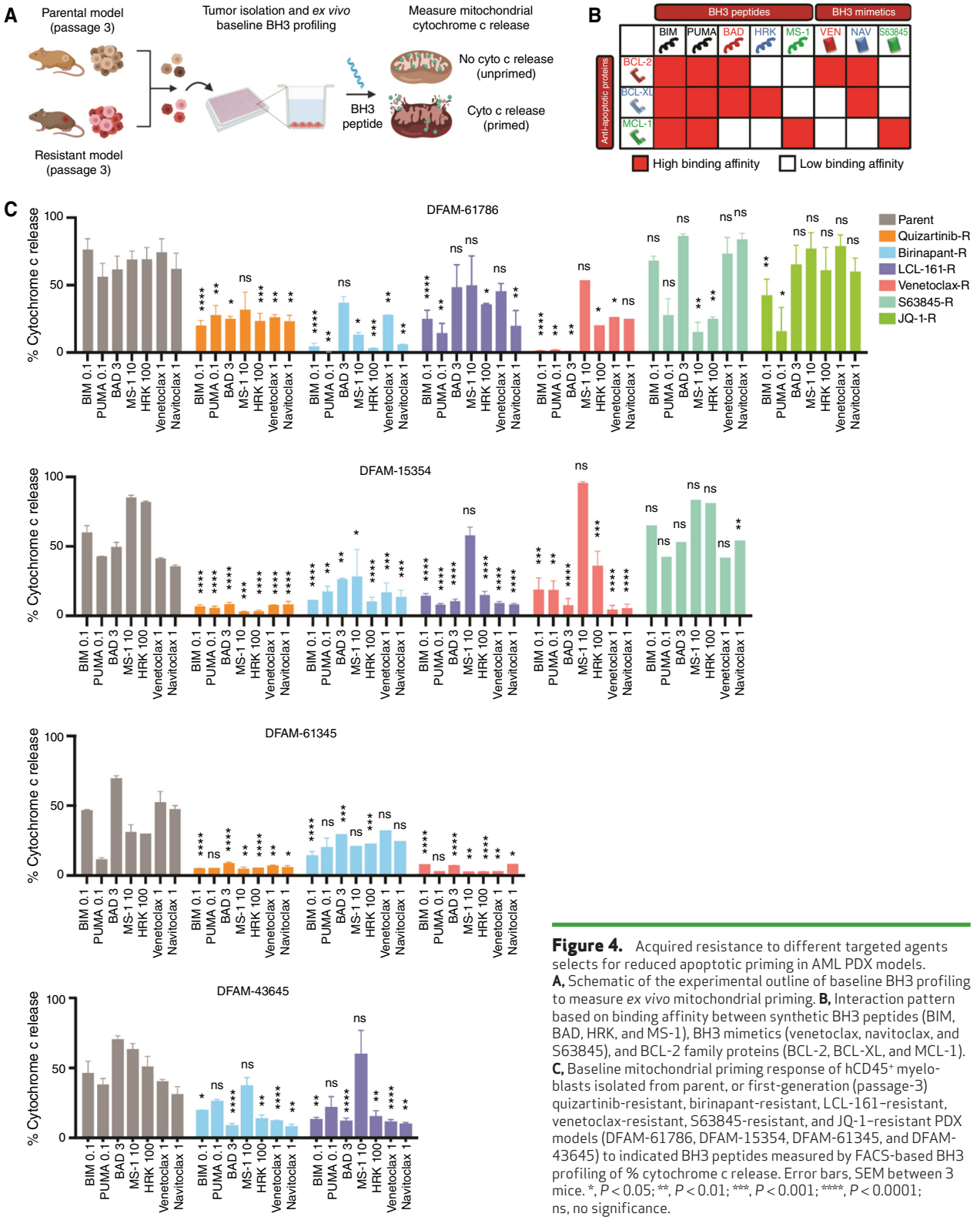

Figure 4. Acquired resistance to different targeted agents selects for reduced apoptotic priming in AML PDX models. **A,** Schematic of the experimental outline of baseline BH3 profiling to measure *ex vivo* mitochondrial priming. **B,** Interaction pattern based on binding affinity between synthetic BH3 peptides (BIM, BAD, HRK, and MS-1), BH3 mimetics (venetoclax, navitoclax, and S63845), and BCL-2 family proteins (BCL-2, BCL-XL, and MCL-1). **C,** Baseline mitochondrial priming response of hCD45$^+$ myeloblasts isolated from parent, or first-generation (passage-3) quizartinib-resistant, birinapant-resistant, LCL-161–resistant, venetoclax-resistant, S63845-resistant, and JQ-1–resistant PDX models (DFAM-61786, DFAM-15354, DFAM-61345, and DFAM-43645) to indicated BH3 peptides measured by FACS-based BH3 profiling of % cytochrome c release. Error bars, SEM between 3 mice. *, $P < 0.05$; **, $P < 0.01$; ***, $P < 0.001$; ****, $P < 0.0001$; ns, no significance.

we next wanted to understand if gene-expression changes in BCL-2 family proteins contribute to this altered mitochondrial apoptotic phenotype. We compared the expression of BCL-2 family genes between parents and myeloblasts resistant to quizartinib, birinapant, and JQ-1. Although we might have expected to find reduced expression of proapoptotic genes or increased expression of their antiapoptotic counterparts in the resistant myeloblasts, we instead found no consistent pattern of mRNA expression changes (Supplementary Fig. S4A–S4C). Next, we performed immunoblotting

to determine whether changes in protein expression among BCL-2 family proteins may cause altered mitochondrial apoptotic phenotypes. We observed downregulation in proapoptotic BAK and BAX for DFAM-61786 and DFAM-61345 PDXs along with upregulation of antiapoptotic MCL-1 in DFAM-61786 (Supplementary Fig. S4D). Of note, these changes appeared mostly consistent across different drugs, irrespective of the underlying mechanism of resistance. DFAM-15354 demonstrated upregulation in BCL-2 and drug-specific changes in BAX and BAK levels (Supplementary Fig. S4D). These findings suggest that protein expression is heterogeneous, but trends across PDXs underscore that BCL-2 family protein levels could act as a determinant of altered mitochondrial apoptotic phenotypes but in a patient-specific manner.

In Vivo Acquired Resistance to Targeted Therapy Selects for MDR

Because we found a selection for reduction in apoptotic priming at acquired resistance irrespective of the mechanism of the initial drug, we next hypothesized that the reduced baseline apoptotic priming would result in a multidrug resistant phenotype. A strong test of this hypothesis requires the testing of many drugs of different classes, a test that would be infeasible if not for modeling with PDX models *in vivo*. We used this far more tractable technique to query drug sensitivity across 40 agents in 16 resistance models. We harvested myeloblasts from spleen and bone marrow of DFAM-61786, DFAM-15354, and DFAM-61345 models (passage-3) before and after they acquired resistance to 6 different targeted therapies (quizartinib, venetoclax, S63845, birinapant, LCL-161, and JQ-1; Fig. 5A). Bone marrow- or spleen-derived myeloblasts from each drug-resistant and matched parental PDX model (n = 22 models, 3 mice/model) were incubated with 40 drugs. The number of drugs tested across different models varied due to a limitation in the number of cells harvested from drug-resistant models. At 14 hours after drug exposure, cells were permeabilized and exposed to BH3 peptides to compare delta priming response in resistant versus parental myeloblasts (Fig. 5A). We found that acquired resistance to quizartinib selected for an MDR phenotype, indicated by a loss in drug-induced mitochondrial priming response to >50% of drugs on the panel across all three PDXs compared with parental PDXs (Fig. 5B). A similar trend was observed for venetoclax-, S63845-, birinapant-, and JQ-1-resistant models for all three PDX models. This suggested that when a particular PDX model or patient acquires resistance to one targeted therapy, they not only lose response to that drug but also to a wide variety of drugs that kill via the mitochondrial pathway of apoptosis. However, the breadth of the MDR may vary from drug to drug. Although we acknowledge that engraftment may cause some migration of the sensitivity profiles of PDX tumors away from the original tumor, a huge advantage of PDX models is to serve as a source of tumor material that we can subject to DBP and *in vivo* drug testing.

Although resistant cells had fewer hits compared with parent cells, we still identified drugs that significantly primed resistant cells (Fig. 5B). Hence, we next asked whether resistant myeloblasts acquired new vulnerabilities, or if they maintained persistent vulnerabilities, by plotting the delta priming response from resistant PDX models with matched parental model (Supplementary Fig. S5A–S5F). Notably, acquired resistance to quizartinib yielded retention of sensitivity to AZD 5991 (MCL-1) and venetoclax (BCL-2) across all models and vemurafenib (BRAF) in two out of three models. All resistant models were also sensitized to panobinostat (HDAC) apart from S63845-resistant PDXs. Acquired resistance to birinapant and LCL-161 yielded a retention of sensitivity to BH3 mimetics (venetoclax, AZD 5991, and S63845), and FLT-3 inhibitors (quizartinib, gilteritinib, and sorafenib). As we previously reported, we saw that acquired resistance to venetoclax and S63845 yielded a retention of sensitivity to FLT-3 inhibitors (quizartinib, gilteritinib, and sorafenib), SMAC mimetics (birinapant and LCL-161), and for venetoclax resistance, MCL-1 inhibitors (S63845 and AZD 5991; ref. 20). Acquired resistance to venetoclax, quizartinib, S63845, JQ-1, birinapant, and LCL-161 yielded generally reduced sensitivity to kinase inhibitors (dasatinib, imatinib, and ruxolitinib) and MK2206 (AKT) respective to other drugs (Supplementary Fig. S5A–S5F). We found that most drugs, apart from <10%, that increased mitochondrial priming of resistant myeloblasts also increased priming of parental myeloblasts, indicating maintenance of persistent drug vulnerabilities found at the preexisting stage rather than identification of novel drug vulnerabilities in the resistant state.

Because we were able to identify MDR phenotypes in PDX models, we next asked, do similar phenotypes exist in humans with acquired drug resistance? To test this, we utilized the data set generated by Malani and colleagues to compare *ex vivo* drug-sensitivity responses to 513 drugs measured via *ex vivo* drug sensitivity and resistant testing (DSRT) in 134 patients with AML (Fig. 5C; ref. 29). Drug responses are depicted as selective drug-sensitivity score (sDSS), calculated as the area under the dose-response curve for patient samples normalized by that of healthy controls. Comparison of *ex vivo* drug sensitivity with the top 40% of scored drugs (defined as >8.7 sDSS) between patients at diagnosis (n = 81) and relapse (n = 53) showed a remarkably high number of effective drugs at diagnosis compared with the relapsed setting (39.7% vs. 18.8%, Fig. 5D; Supplementary Fig. S6A and S6B). To determine the classes of drugs that lost response at relapse, we derived normalized *ex vivo* drug sensitivity for each class of agents. Drugs targeting kinases (PI3K, mTOR, MEK, JAK, and Aurora) and HDAC showed selective loss of response in patients at relapse (Fig. 5E; Supplementary Fig. S6C). Further, we also observed a notable reduction in the percent of patients who responded to the top 40% of scored drugs (defined as >8.7 sDSS) between diagnosis and relapse (41.8% of patients responded in diagnosis compared with 30.6% in relapse, Fig. 5F). Thus, we determined that patients with AML do broadly lose sensitivity to agents in a similar MDR manner as drug-resistant PDX models. We next performed drug-by-drug comparison of *ex vivo* sensitivity in the relapsed versus diagnosis patient tumors in two large data sets: Helsinki study (ref. 29; 513 compounds) and Beat AML study (refs. 28, 30; 164 compounds). Note that we did not do a paired-wise comparison due to limited paired samples. Nonetheless, we found that >60% of the drugs showed greater *ex vivo* drug-sensitivities (sDSS) on diagnosis samples compared with

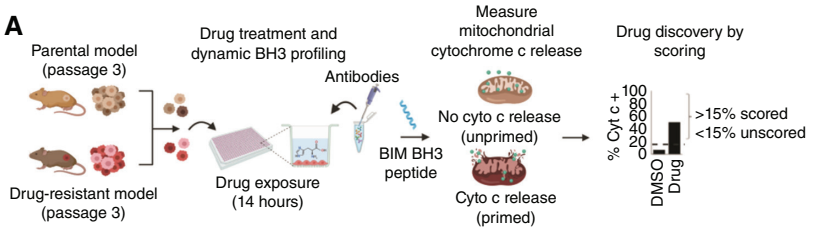

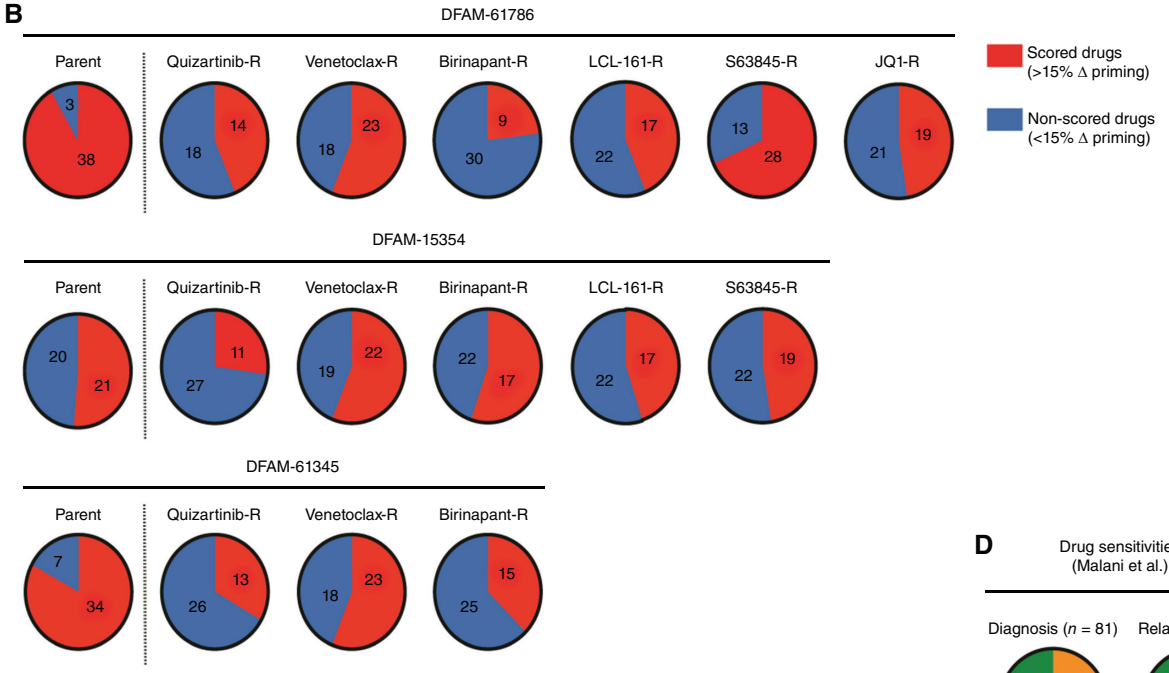

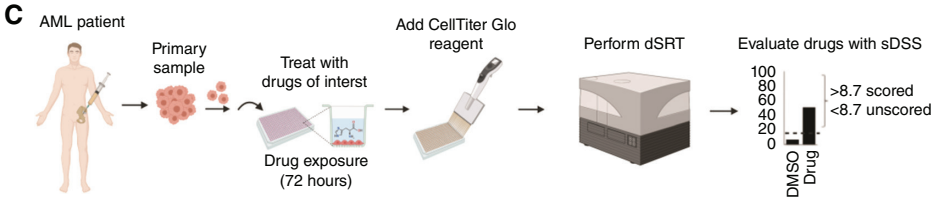

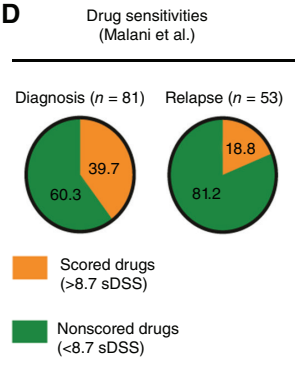

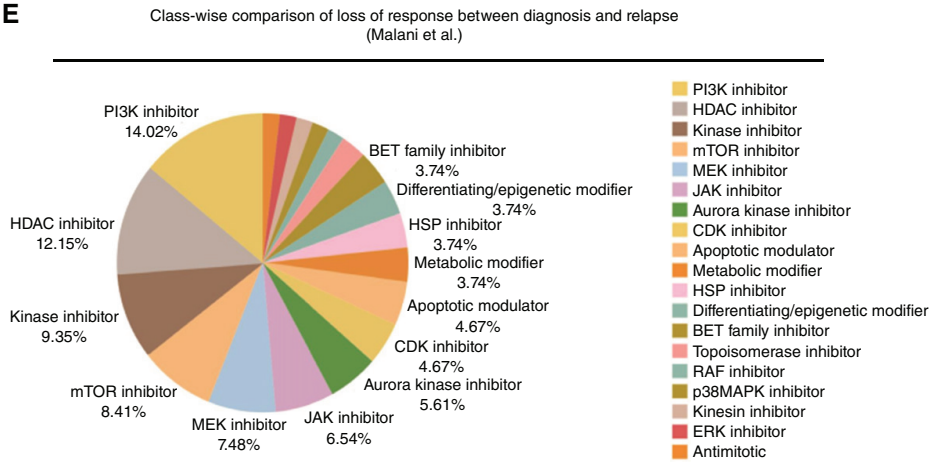

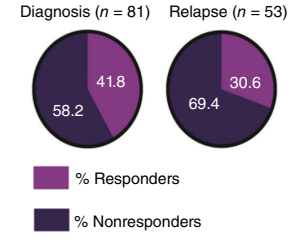

R/R cases (Supplementary Fig. S7A and S7B). As expected, a much smaller cohort of drugs showed higher *ex vivo* sensitivity (sDSS) in R/R patients as compared with the diagnosis, indicating a trend for persistent vulnerability as opposed to relapsed-specific sensitivity.

Ex Vivo DBP Identifies *In Vivo* Responses to Single Agent Therapy in AML PDXs

Above, we relied on DBP to identify drug sensitivities in treatment-naïve and relapsed contexts. To validate that DBP accurately mirrors *in vivo* drug sensitivity, we tested *in vivo* sensitivity to 5 drugs of disparate mechanisms of action: birinapant and LCL-161 (SMAC mimetics), JQ-1 (BRD-4 inhibitor), venetoclax (BCL-2 antagonist), and quizartinib (FLT-3 inhibitor) in 4 to 9 different PDX models each. These drugs were selected based on their clinical relevance, pharmacokinetics, and range of priming responses measured by *ex vivo* DBP (Supplementary Fig. S8A). NSG mice engrafted with primary AML cells (passage-2) were enrolled in the study when the circulating blast count exceeded 5% in peripheral blood (Supplementary Fig. S8B). The animals were randomly divided into vehicle and treatment groups (n = 5/model/therapy) and therapy was continued for 2 weeks, after which circulating blast counts were measured to assess leukemia burden (Fig. 6A). As expected, there was heterogeneity of response to drugs across different PDX models (Fig. 6B). Using *ex vivo* DBP assay, we identified drugs that prime not only treatment-naïve PDXs but also R/R PDXs (Fig. 6B). For instance, R/R PDXs DFAM-61345, DFAL-49600, and DFAM-58159 are sensitive to venetoclax; DFAM-58159 and DFAM-33766 are sensitive to birinapant; DFAM-61345, DFAL-49600, and DFAM-33766 are sensitive to quizartinib (Fig. 6B). To further test the predictive power of DBP, we compared the delta priming measured on myeloblasts isolated from PDXs with the peripheral blast reduction at day 15 after treatment (Fig. 6C; Supplementary Fig. S8B). In each case, *ex vivo* DBP significantly predicted *in vivo* response—the greater the drug-induced changes in apoptotic priming observed, the better the *in vivo* response (Fig. 6C). Despite *ex vivo* mitochondrial sensitivity, MSK-777 (CDC-7 inhibitor) and JIB-04 (KDM4A inhibitor) failed to show substantial *in vivo* activity due to high toxicity and poor pharmacodynamic activity, respectively (Supplementary Fig. S8C–S8F).

Next, we wanted to test whether mitochondrial priming measured by *ex vivo* DBP can stratify the activity of FLT-3 inhibitors in AML PDXs according to the genetic status of *FLT-3*. We performed DBP on *FLT-3-ITD*$^+$ (MOLM-13, MOLM-14, and MV4-11) and *FLT-3-ITD*$^-$ (U937 and OCI-AML-3) AML cell lines. *FLT-3-ITD*$^+$ cell lines showed increased delta priming to proapoptotic BH3 peptides in response to FLT-3 inhibitors (quizartinib, gilteritinib, sorafenib, and midostaurin) compared with *FLT-3-ITD*$^-$ cell lines (Supplementary Fig. S9A). Further, cell viability assays confirmed that DBP can predict increased cytotoxicity of FLT-3 inhibitors in *FLT-3-ITD*$^+$ cell lines (Supplementary Fig. S9B). Next, we utilized AML PDXs to evaluate whether DBP could predict *in vivo* response to FLT-3 inhibitors. DBP predicted quizartinib activity not only in *FLT-3-ITD*$^+$ mutated PDXs but also in PDXs carrying mutations other than the ITD region of FLT-3 and WT FLT-3 (Fig. 6C; Supplementary Fig. S9C–S9E). We then tested R/R FLT-3 mutant AML human samples (n = 7) derived from the clinical trial of an FDA-approved FLT-3 inhibitor, gilteritinib (5), to test the clinical utility of DBP in predicting response. We found that pretreatment myeloblasts of patients who showed an enhanced priming response to gilteritinib via DBP at 14 hours indeed achieved an objective complete remission ($P < 0.05$; Fig. 6D). Of note, IDH1/2 inhibitors ivosidenib and enasidenib did not substantially enhance mitochondrial priming (<15%) in IDH1/2 mutant AML PDXs (Supplementary Fig. S9F).

In clinical practice, response is often considered categorically rather than as a continuous parameter. To test the performance of DBP as a categorical predictor of *in vivo* response, we classified response as ≥50% reduction in blast counts in PDX models and then performed a receiver-operating characteristic (ROC) curve analysis using all five diverse pathway inhibitors tested *in vivo*. DBP was a good binary predictor of *in vivo* responses in AML PDXs (AUC of the ROC curve of 0.84, $P < 0.01$; Fig. 6E). Thus, DBP performed well as a predictive biomarker in AML PDX models across drugs of divergent mechanisms of action.

DBP Identifies Targeted Therapy for Quizartinib-Resistant PDX Models

We finally asked whether drugs that retained the ability to increase mitochondrial priming in drug-resistant myeloblasts could overcome *in vivo* acquired resistance. To prioritize compounds for *in vivo* study, we searched for drugs that increased priming in both the parent and quizartinib-resistant DFAM-61786 PDX models (Fig. 7A). We tested *in vivo* efficacy of five drugs: venetoclax, birinapant, quizartinib, S63845, and vemurafenib, which showed >15% delta priming in *ex vivo* DBP assays on quizartinib-resistant myeloblasts (Fig. 7B). We serially transplanted quizartinib-resistant cells into new NSG mice (n = 5 mice/group) and measured peripheral blasts every week. For quizartinib-resistant mice, we found that treatment with birinapant, venetoclax, and S63845, which showed the greatest drug-induced changes

Figure 5. Acquired resistance to targeted therapy selects for multidrug resistance phenotypes in AML PDX models and clinical patients. **A,** Schematic of the drug discovery process in resistant PDX models using *ex vivo* DBP. **B,** Pie charts of DBP results comparing delta priming responses in myeloblasts derived from parental and quizartinib-, venetoclax-, birinapant-, LCL-161-, S63845-, and JQ-1-resistant PDXs (DFAM-61786, DFAM-15354, and DFAM-61345) in response to different targeted drugs. Drugs that induced >15% increase in mitochondrial delta priming were categorized as scored drugs. **C,** Schematic of *ex vivo* drug sensitivity response testing (DSRT) to assess selective drug-sensitivity scores (sDSS) in AML primary tumors treated with drugs of interest. **D,** Pie charts comparing sDSS of 513 targeted therapies in AML primary tumors derived from patients at diagnosis with patients at relapse from Malani et al. (29). Drugs that showed >8.7 sDSS by DSRT assay were categorized as a scored drug. Refer to Supplementary Fig. S6 for individual drug sensitivity in each patient. **E,** Pie chart of class-wise distribution for drugs that showed selective drug-sensitivities (sDSS > 8.7) in only AML primary tumors from patients at diagnosis, not at relapse, from Malani et al. (29). Percentage signifies the number of drugs from each class losing activity in the relapsed setting, in comparison to the total number of drugs (n = 513) administered. **F,** Pie charts comparing response rate of AML primary tumors to 513 drugs using DSRT assay in patients at diagnosis versus relapse (normalized), from Malani et al. (29).

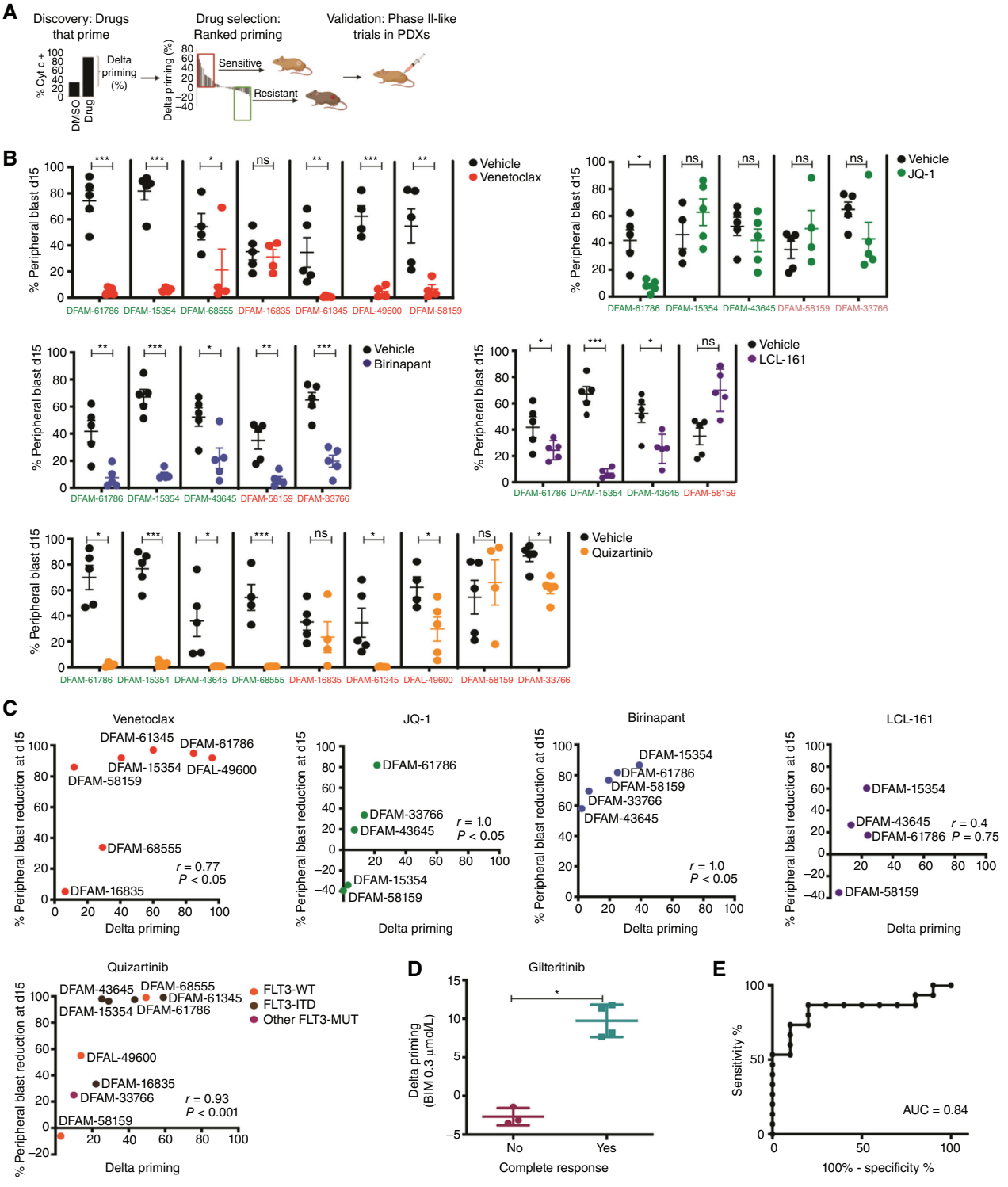

Figure 6. DBP as a binary predictor of *in vivo* response to AML-targeted therapy in PDX models. **A,** Experimental schematic for drug selection and validation in PDX models. **B,** NSG mice injected with 0.6 million primary AML cells (passage-2) were subjected to 2 weeks of treatment when circulating blast count >10% in peripheral blood. Plotted are the % hCD45$^+$ leukemic cells in the peripheral blood at day 15 after treatment. Each dot indicates a mouse; green = treatment-naïve PDX; red = R/R PDX; line indicates mean ± SEM; statistical analysis by two-tailed Student *t* test. **C,** Spearman correlation between delta priming obtained by *ex vivo* DBP on myeloblasts and % blast reduction at day 15 after therapy. FLT-3 mutation status of each PDX model is represented. **D,** Delta priming response to gilteritinib (FLT-3 inhibitor) derived from DBP using BIM peptides in pretreatment myeloblasts compared with clinical response status of FLT-3-mutated AML patients treated with gilteritinib. Horizontal line is the median with interquartile range bars; statistical analysis by one-tailed Wilcoxon-rank test. *, $P < 0.05$. **E,** Receiver-operating characteristic curve (ROC) analysis of AML PDXs in response to 6 different targeted agents, demonstrating the predictive power of *ex vivo* DBP (AUC = 0.84, $P < 0.01$); statistical analysis by Mann-Whitney U test. *, $P < 0.05$; **, $P < 0.01$; ***, $P < 0.001$; ns, no significance.

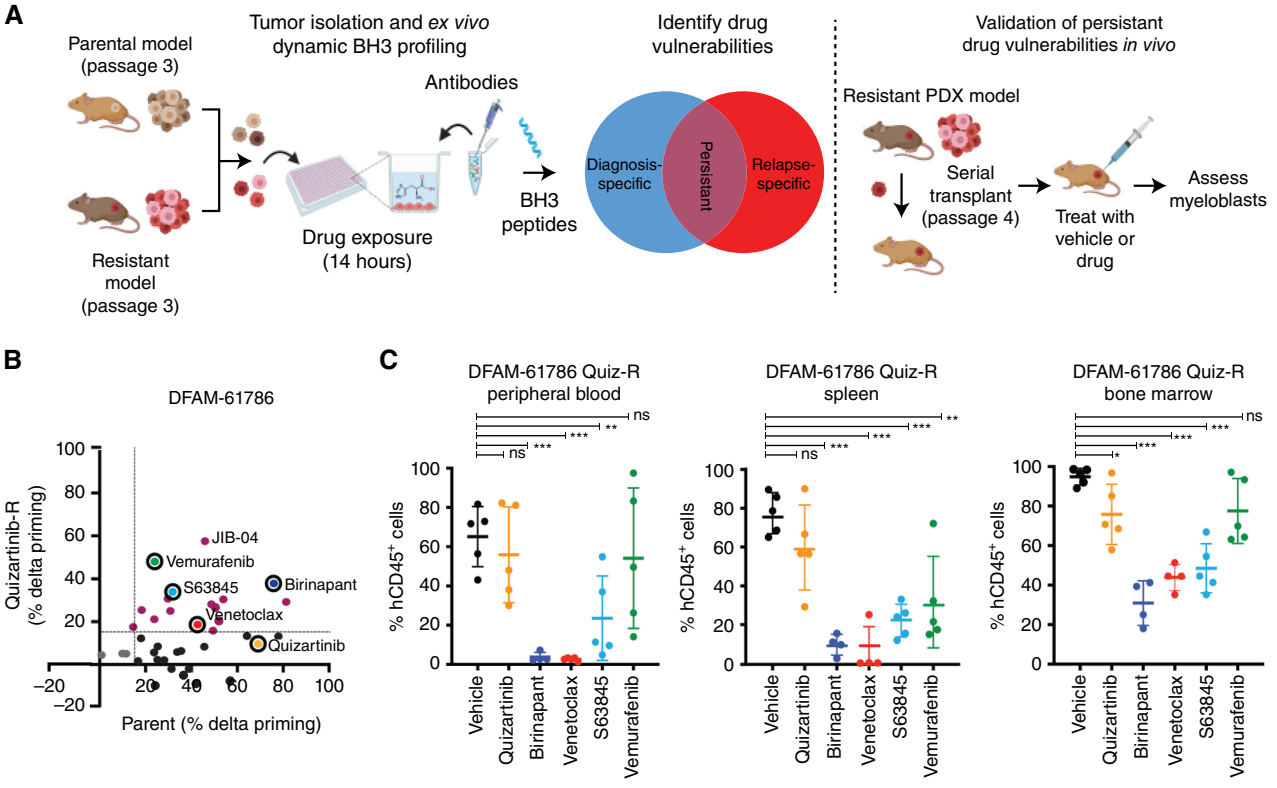

Figure 7. DBP identifies targeted therapy for quizartinib-resistant disease. **A,** Schematic of experimental strategy for DBP-based discovery of drugs that induce priming for apoptosis in quizartinib-resistant PDX DFAM-61786 (passage-3), followed by *in vivo* validation of the strategy with drugs of interest. **B,** Comparison of delta priming response from *ex vivo* DBP of parent vs. quizartinib-resistant DFAM-61786 ($n = 3$ mice/group) is shown. Drugs of interest that maintained the ability to prime for apoptosis by inducing >15% delta priming in the quizartinib-resistant setting are highlighted purple. X-axis = parent, y-axis = quizartinib-resistant. **C,** 0.6 million resistant myeloblasts from PDX DFAM-61786 were serially implanted into NSG mice and assigned into 6 treatment arms ($n = 5$ mice/group). Shown are the %hCD45$^+$ blast counts in peripheral blood, spleen, and bone marrow in response to drugs that showed increased priming via DBP in **B:** venetoclax, S63845, birinapant, and vemurafenib. Quizartinib was used as a negative control. JIB-04 was not assessed in quizartinib-resistant mice due to low pharmacodynamic activity *in vivo*. Each dot indicates a mouse; the line indicates mean ± SEM; *, $P < 0.05$; **, $P < 0.01$; ***, $P < 0.001$; ns, no significance; one-way ANOVA. (*continued on next page*)

in apoptotic priming, was indeed able to significantly reduce myeloblasts compared with vehicle treatment in all three compartments, whereas vemurafenib showed spleen-specific antileukemic activity (Fig. 7C). As expected, animals receiving quizartinib failed to inhibit leukemia progression. To evaluate molecular changes that may contribute to drug resistance, we also performed immunoblotting assays. Supportive to transcriptomic signatures, quizartinib-resistant myeloblasts from the DFAM-61786 model showed persistent phosphorylation of FLT-3 and enhanced activation of JAK–STAT and MAPK signaling, indicated by increased levels of pSTAT-5 and pERK (Supplementary Fig. S10A and S10B). Note that although it may have been of great utility to identity the acquisition of novel pathway dependencies, we did not detect newly acquired drug sensitivities specific to resistant myeloblasts in this model.

Next, we compared *ex vivo* selective drug-sensitivity scores (sDSS) in patients with AML at diagnosis versus relapse for the 28 drugs (Helsinki study) and 24 drugs (Beat AML study) that overlapped with 40 targeted agents that were tested on our acquired resistant AML PDXs (Fig. 7D and E). In agreement with our findings from PDX models, both studies revealed persistent or increased activity of birinapant and LCL-161 (IAP antagonist), venetoclax (BCL-2i), and vemurafenib (B-Rafi), in the Helsinki and Beat AML data sets (28–30). Beat AML patients also showed persistent/higher sensitivity to quizartinib (FLT-3) and panobinostat (HDAC) in R/R patients compared with diagnosis (Fig. 7D and E). This key finding suggests that *ex vivo* DBP could be applicable to choose therapy for patients with R/R AML.

DISCUSSION

The majority of patients diagnosed with AML die of their disease, despite the availability of active standard chemotherapy regimens, targeted therapies, and allogeneic transplantation. Thus, there is an urgent need to understand how drug sensitivity changes over the course of treatment, how to predict the best treatment strategies to achieve long-term remission, and what molecular changes drive leukemia relapse.

Although the development of drug resistance is likely a multifactorial phenomenon, we showed that selection for reduced mitochondrial apoptotic priming nearly invariably accompanies the acquisition of resistance to numerous narrowly targeted agents, as we showed previously for conventional chemotherapy (27, 38). Note that this happened in

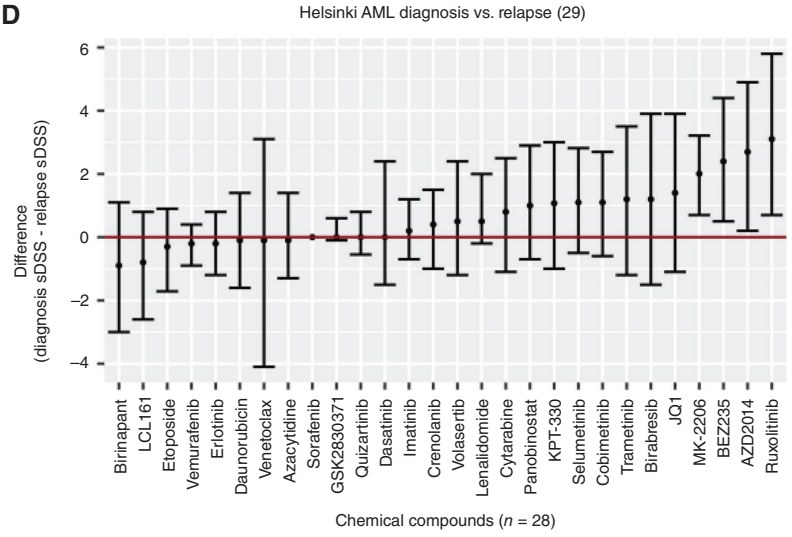

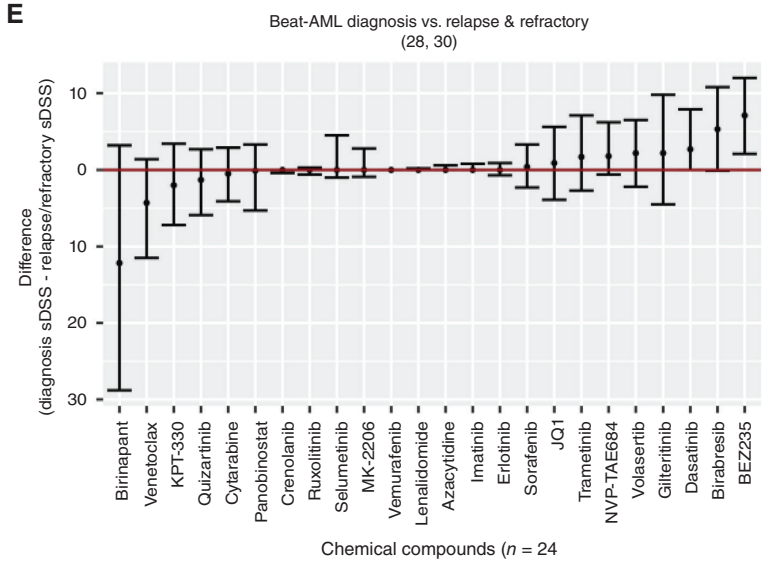

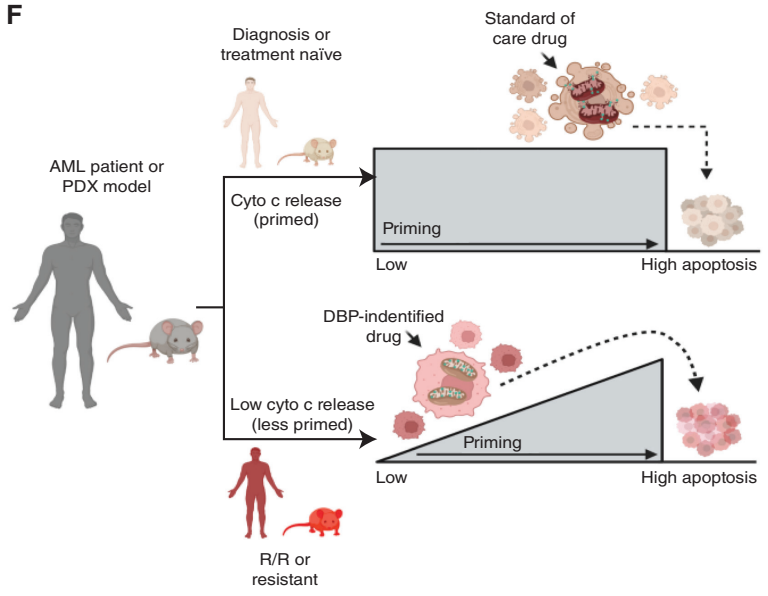

Figure 7. ***(Continued)*** **D,** Comparison of selected compounds (that shows overlap with drugs tested in **B**) sensitivity scores (sDSS) in diagnosis vs. relapse Helsinki cohort (29) and diagnosis versus R/R Beat AML cohort (**E**; 28, 30). For each drug, sDSS scores of diagnosis cases were compared against sDSS scores for R/R cases using the Mann–Whitney *U* test. The estimated difference between the two sample groups and 95% confidence interval were obtained and plotted in the error bar chart. **F,** Schematic for reduction in mitochondrial priming as a proposed model of acquisition of drug-resistance in the AML model.

the setting of frequent, though not invariable, selection for increased expression of drug metabolism and drug efflux genes (Fig. 3F). This is an important reminder that even if target-specific resistance mechanisms can be identified, there is likely simultaneous selection for broad resistance mechanisms that confer the MDR all too commonly observed in relapsed cancers. The importance of reduced mitochondrial apoptotic priming in causing MDR can be inferred from the S63845-resistant (DFAM-16835 and DFAM-15334) models. These resistant models did not show a reduction in baseline apoptotic priming (Fig. 4C). They are also the only resistant models that did not demonstrate a broad loss of sensitivity to the many drugs in our platform (Fig. 5B). Further, our genomic studies critically provide evidence that drug resistance can arise even in the absence of genetic mutations, which challenges the previous literature that widely shows that relapse is mostly driven by genetic mutations during drug treatment (39, 40).

Although genetics doubtlessly contributes to resistance in many cases (13–15, 41), resistance to venetoclax (20, 42, 43), S63845, birinapant, and JQ-1 was acquired in the absence of new genetic mutations in leukemia-related genes. However, quizartinib-resistant PDX models showed the acquisition of new genetic mutations and changes in VAF for existing mutations in three of five PDX models (Supplementary Fig. S11A–S11C). Our RNA-seq data emphasize that there are nongenetic mechanisms behind drug resistance, such as reduced mitochondrial priming, upregulation of ABC transport genes, and enrichment of drug-specific transcriptomic signatures. Such mechanisms have yet to be deeply studied and remain novel in nature. Moreover, we also emphasize that these nongenetic mechanisms behind drug resistance may be therapeutically exploited. We discovered that loss in mitochondrial priming may not be associated with a consistent corresponding increase in either antiapoptotic genes or a decrease in proapoptotic genes at transcript levels but rather associated with the protein levels of BCL-2 family members. This may suggest that posttranslational modifications, functional dependence on prosurvival versus prodeath BCL-2 family proteins, molecular changes in mitochondrial structure, or biogenesis might play a role in driving reduced apoptotic sensitivity upon acquisition of relapse. Overall, although we think it is likely that both genetic and nongenetic changes contribute to the evolution of resistant clones, our results suggest that selection for reduced apoptotic priming may be an important nongenetic selection pressure governing the emergence of resistant populations. Indeed, it may be that combinations that include direct apoptotic modulators would present a viable strategy to treat patients with relapsed AML by enhancing overall apoptotic priming (Fig. 7F).

One avenue to improved patient therapy is the rapid and personalized identification of more active drugs. MDR associated with a reduced sensitivity to apoptosis is a clinically ominous finding. By detecting functional dependence, DBP has the important advantage that it can rapidly predict response to inhibitors for which no genetic biomarkers exist based on the mitochondrial apoptotic sensitivity of leukemia cells. We found that across a myriad of drugs with diverse mechanisms of action, DBP provided an excellent predictor of *in vivo* response. Here (Fig. 5D), and elsewhere (20, 44, 45), we have found that DBP can predict response in human patients. Others have recently used different functional methods, exposing patient cells to a panel of drugs, to demonstrate their ability to identify active therapy in the clinic as well (28–30, 46, 47). A potential advantage of DBP is that it may identify agents that selectively increase mitochondrial priming of AML cells but are not sufficient to kill as single agents. However, such agents, not identifiable by other functional testing methods nor by genetic biomarkers, may nonetheless become extremely valuable in designing combination therapies. DBP may also be used to help classify mechanisms of action for novel agents where mechanisms are unknown by examining nearest neighbor drugs, as in Supplementary Fig. S12A.

It is an attractive idea that resistance to one agent may actually reveal an enhanced vulnerability to another, a new "Achilles heel." However, while admitting the desirability of such an outcome, this is not what we observed in our study with our screening panel (40 agents). This suggests to us that whereas we cannot rule out the existence of such acquired vulnerabilities, they may be rare and difficult to find. In studies carried out by other groups that utilized larger panels of drugs (Helsinki and Beat AML), such acquired vulnerabilities were sometimes identified, suggesting that very broad screening strategies might be necessary to identify them (28–30). In sum, given these compelling preclinical findings, we are developing a prospective phase II DBP-guided trial to select therapies for patients with R/R AML.

METHODS

Human Subjects

All AML patient samples and healthy donor samples were obtained after written informed patient consent under collection protocols approved by Dana-Farber Cancer Institute IRB and the National University of Singapore DSRB. The study was conducted in accordance with recognized ethical guidelines (e.g., Declaration of Helsinki, CIOMS, Belmont Report, U.S. Common Rule). We have included patient demographic characteristics for age, gender, race, and ethnicity when the information was available in Supplementary Table S1 (48, 49).

PDX Models and In Vivo *Study*

All animal studies were performed in accordance with approved Institutional Animal Care and Use Committee (IACUC) guidelines at Dana-Farber Cancer Institute animal facility (IACUC protocol #14-038) and at the National University of Singapore facility (IACUC protocol # R20-0342). AML PDX models are available from the Center for Patient-Derived Models at Dana-Farber Cancer Institute (https://www.pdxfinder.org/source/dfci-cpdm/; ref. 32). Female NSG mice at 6 to 8 weeks of age (The Jackson Laboratory) were injected with 0.6 million human leukemia cells intravenously (i.v.). Following transplant, mice were bled weekly, and treatment was initiated when the circulating leukemia burden was >5% as assessed by flow cytometry staining for hCD45 (clone HI30, BD Biosciences) and hCD33 (clone WM53, BD Biosciences). All blood samples were lysed with ammonium chloride red-blood-cell buffer (Qiagen) prior to staining.

Animal Treatments

Clinical-grade venetoclax (Medchem express) was formulated in a mixture of 60% phosal 50 PG, 30% PEG 400, and 10% EtOH and administered 100 mg/kg per os (p.o.) 5 days per week. Quizartinib (Selleckchem) was formulated in 22% hydroxypropyl-β-cyclodextrin

(Sigma-Aldrich, C0926) and administered 20 mg/kg intraperitoneally (i.p.) 5 days per week. Birinapant (TargetMol Inc.) was formulated in citrate buffer (pH 5.5) and administered 5 mg/kg i.p. 3 days per week. JQ-1 was formulated in 10% hydroxypropyl-β-cyclodextrin and administered 50 mg/kg i.p. 5 days per week. S63845 was kindly provided by Servier/Novartis, was formulated in 2% vitamin E/TPGS in 0.9% NaCl, and was administered 25 mg/kg i.v. 2 days per week (note: this dose is reduced from the original due to tail necrosis from continuous i.v. exposure). LCL-161 was kindly provided by Novartis, was formulated in 30% of 0.1N HCl and 70% of 100 mmol/L sodium acetate buffer at pH 4.5, and was administered 100 mg/kg p.o. 4 days per week.

Lineage Depletion and CD34⁺ Isolation

Human mononuclear cells obtained from healthy donor apheresis samples (n = 3) were isolated using a Ficoll gradient. Samples underwent lineage depletion using Miltenyi Biotec's human lineage cell depletion kit following the manufacturer's directions. The purity of the remaining population was determined by staining with human CD34 antibody and quantified via flow cytometry. Cells were cultured in 24-well plates at a density of 50,000/mL in StemSpan SFEM II media with 1% penicillin/streptyomycin, and 1 nmol/L StemRegenin 1 (Stem Cell Technologies) and subjected to drug treatment followed by DBP.

BH3 Profiling and DBP

Animals were humanely euthanized, and the spleen and bone marrow were processed into single-cell suspensions. Red blood cell lysed cells were plated with heat-inactivated RPMI-1640 (Invitrogen) and 10% fetal bovine serum in 24-well plates at 1 million/mL and exposed to a panel of targeted agents for 14 hours or DMSO (control) followed by BH3 profiling (50). BH3 profiling involves determining sensitivity to BH3 peptides without drug perturbation, whereas DBP determines sensitivity after exposure to drugs (23, 50). Briefly, cells were exposed to synthetic BH3 peptides after plasma membrane permeabilization by 5% digitonin. The gating strategy included antibody markers for CD45 (Fisher Scientific, Clone HI30), CD34 (BioLegend, Clone 581), CD38 (BioLegend, Clone HIT2), CD33 (Fisher Scientific, Clone WM53), c-kit (BioLegend, Clone 104D2), and live/dead fixable zombie yellow stain (BioLegend). AML blasts were identified by CD45 lo-mid/SCC-low. Sensitivity to BH3 peptides was measured as percent cytochrome c release (BioLegend, 6H2.B4) loss as determined by FACS. A gate was drawn around the DMSO-negative control (alamethicin) to depict 100% cytochrome c retention. DMSO was used as a negative control for cytochrome c release, whereas a control without the cytochrome c antibody was used as a positive control for 100% cytochrome c release. In BH3 profiling, cytochrome c loss was calculated using the following equation: [cytochrome c loss = 100 − (% of cells within cytochrome c retention gate)]. The readout of DBP is a drug-induced change in priming defined as "delta priming" (calculation: delta priming = cytochrome c loss [drug] − cytochrome c loss [DMSO]). An acceptable delta priming threshold (<15%) calculated by cytochrome c release caused by 3 (mean ± SD) of DMSO-treated wells was used to determine significance.

DNA Sequencing

Samples from Dana-Farber Cancer Institute were assessed using CLIA-approved NGS (BWH Rapid Heme Panel) based on the TruSeq Custom Amplicon kit from Illumina. In total, 88 genes were assessed using hotspot codons for oncogenes and entire coding regions for tumor suppressor genes (51), or a specific prepanel to determine the karyotype of mutations using Hemoseq. NUS PDXs were screened with NGS to evaluate for myeloid panels containing *ABL1, ASXL1, ATRX, BCOR, BCORL1, BRAF, CALR, CBL, CBLB, CBLC, CDKN2A, CEBPA, CSF3R, DNMT3A, ETV6, EZH2, FBXW7, FLT3, GATA1, GATA2, GNAS, HRAS, IDH1, IDH2, IKZF1, JAK2, KDM6A, KIT, KRAS, MLL, MPL, MYD88, NOTCH1, NPM1, NRAS, PDGFRA, PHF6, PTEN, PTPN11, RAD21, RUNX1, SETBP1, SF3B1, SMC1A, SMC3, SRSF2, STAG2, TET2, TP53, U2AF1, WT1,* and *ZRSR2.*

RNA-Seq

We measured tumor burden from bone marrow and spleen for selected PDX models shown in Supplementary Table S2. Once engraftment reached >70% in circulation, we proceeded with tissue harvest. We did not enrich for hCD45⁺ cells. mRNA was extracted from fresh or frozen samples with Qiagen's RNeasy Mini Kit following the manufacturer's instructions. Samples were submitted for RNA-seq to MBCF (Molecular Biology Core Facilities) core at DFCI. Briefly, nonstranded RNA-seq libraries were generated using the True-SeqRNA Sample Prep kit (Illumina) on a Sciclone platform (PerkinElmer). mRNA underwent fragmentation, cDNA synthesis, and next-generation library synthesis via exome capture and PCR amplification. Libraries were sequenced on a Next-Seq instrument (Illumina) using a paired-end protocol. Paired-end RNA-seq samples were matched to the human (hg19) and mouse (mm9) genomes with the first STAR (52). Each pair of BAM files were then passed onto Xenofilter to eliminate mouse reads, and resulting BAM files were converted back to fastq files. Transcript expression was quantified using Salmon and was summarized to gene-level. Genes with transcripts smaller than 300 bp were ignored. The count data matrix obtained from Salmon was imported into R using tximport (R package), and then Limma was applied to perform differential analysis. All expression values were $\log_2$ fold transformed. The output from Limma was then used for GSEA, using clusterProfiler to calculate the normalized enrichment score and false discovery rate (FDR). The RNA-seq data for AML patient samples from Malani and colleagues study were processed as shown previously (Ref PMID: 28818039; ref. 29).

Calcein-AM Efflux Assay

Viably frozen PDX cells were thawed and resuspended in RPMI-1640. PDX cells were plated in 24-well plates at 2.5×10^5/mL and exposed to 75 μmol/L verapamil or vehicle for 10 minutes. The cells were then incubated for 20 minutes after the addition of 50 μmol/L calcein-AM. After incubation, the cells were washed, resuspended in HBSS, and stained with CD45 antibody for flow-cytometric analysis. Data were acquired on the BDFACS Celesta cell analyzer, and histograms were generated in FlowJo.

Statistical Analysis

GraphPad Prism version 9.0 was used to perform the following: one-tailed Mann–Whitney-rank sum test to assess the equality of means in diagnosis and relapsed independent samples; two-tailed Student t test to assess response (via percent peripheral blasts at day 15) in vehicle-treated or drug-treated PDXs; Spearman correlation to assess nonparametric magnitude of response between two parameters (*ex vivo* DBP and *in vivo* blast reductions), assuming that data may not be normally distributed; one-tailed Wilcoxon-rank sum test to assess delta priming versus complete clinical response, assuming nonparametric magnitude; unpaired t test to assess drug response (via percent peripheral blasts) vehicle-treated or drug-treated PDXs while developing acquired resistance models; one-way ANOVA to assess the *in vivo* response to five different drugs (quizartinib, birinapant, venetoclax, S63845, and vemurafenib) in quizartinib-resistant DFAM-61786 peripheral blood, spleen, and bone marrow. Selective drug-sensitivity scores (sDSS) for Beat AML data were calculated using Breeze (53). Benjamini–Hochberg method was used to assess first-ordered hypotheses based on P value ($P < 0.05$).

Mice Studies. We utilized a total of 30 PDX model-drug combinations to test the *in vivo* efficacy of PDX models predicted to be sensitive via *ex vivo* DBP. For venetoclax = 7 PDX models, JQ-1 = 5 PDX models,

birinapant = 5 PDX models, LCL-161 = 4 PDX models, quizartinib = 9 PDX models. For our acquired resistance studies, we generated total of 14 drug-resistant models and paired parental model to each drug (venetoclax-resistant = 3, quizartinib-resistant = 3, birinapant-resistant = 3, S63845-resistant = 2, LCL-161–resistant = 2, JQ-1–resistant = 1). We have used 10 mice ($n = 5$ vehicle group + $n = 5$ treatment group) to obtain at least 80% power and an effector size of 60% with $P < 0.05$ for each such model and drug using one-way ANOVA.

qPCR

mRNA was extracted from fresh or frozen samples with Qiagen's RNeasy Mini Kit following the manufacturer's instructions. cDNA was synthesized from mRNA using the Bio-Rad iScript cDNA Synthesis Kit. qPCR was performed on the Bio-Rad CFX96 Touch Real-Time PCR Detection System using the Applied Biosystems TaqMan Fast Advanced Master Mix and predesigned TaqMan Gene-Expression Assays (GAPDH: Hs02786624_g1, ABCB1: Hs00184500_m1, FGFR1: Hs00241111_m1).

Immunoblotting

Viably frozen PDX cells pre- and post-resistance (venetoclax, quizartinib, birinapant, S63845, and JQ-1) were lysed in RIPA buffer (Sigma-Aldrich) for immunoblotting and supplemented with protease inhibitor cocktail and phosphatase inhibitor. Antibodies used included ERK (Cell Signaling Technology; 9102), FLT-3 (Cell Signaling Technology; 3462), Normal Rabbit IgG (Cell Signaling Technology; 2729), p- FLT-3 (Cell Signaling Technology; 4577), P-p44/42 MAPK (Erk1/2; Cell Signaling Technology; 9101), p-STAT-5 (Cell Signaling Technology; 9359), STAT-5 (Cell Signaling Technology; 25656).

Data Availability Statement

Clinical information, including patient age, sex, and genetic mutation, is provided in the Supplementary Table. The source data associated with each figure are provided in the manuscript. Normalized FPKM value and FASTQ files for RNA-seq data are deposited under the accession number GSE237794. Raw sequence reads for targeted exome sequencing, and all other data supporting the findings of this study are available from the corresponding authors upon reasonable request.

Code Availability

The RNA-seq data analysis was performed in R. The pathway analyses for differentially regulated genes were performed using the KEGG pathway analysis. All computer code is available upon reasonable request.

Authors' Disclosures

M.S. Pioso reports grants from NIH during the conduct of the study. B. Yilma reports being a full-time employee of Tempus AI since February 2023 and is set to receive restricted stock units in 2024. However, Yilma's time at Tempus and the work presented here (and contributions made during Yilma's time at Dana-Farber Cancer Institute, 2017–2019) did not overlap in any way. J.A. Ryan reports personal fees from Zentalis outside the submitted work; in addition, J.A. Ryan has a patent for BH3 profiling issued, licensed, and with royalties paid from Zentalis. M.R. Luskin reports other support from AbbVie, personal fees and other support from Novartis, and personal fees from KITE and Jazz outside the submitted work. O. Kallioniemi reports other support from Sartar Therapeutics, grants and personal fees from Knut and Alice Wallenberg Foundation, personal fees from Novo Nordisk Foundation, and grants from Sigrid Juselius Foundation outside the submitted work. D.M. Weinstock reports other support from Merck and grants from Astra-Zeneca during the conduct of the study, other support from Merck, and grants from Daiichi-Sankyo outside the submitted work. J.S. Garcia reports grants, personal fees, and other support from AbbVie, personal fees and other support from Genentech, personal fees from BMS and Servier, other support from Pfizer, and other support from Prelude outside the submitted work. A. Letai reports personal fees from Trueline Therapeutics, Zentalis Pharmaceuticals, Flash Therapeutics, and Astra-Zeneca outside the submitted work, and BH3 profiling was employed in this work. There is a portfolio of patents that are owned by his employer, Dana-Farber Cancer Institute, on which he is an inventor. S. Bhatt reports grants from the National Medical Research Council, the American Society of Hematology, and the Claudia-Adams Barr Foundation during the conduct of the study. No disclosures were reported by the other authors.

Authors' Contributions

E.A. Olesinski: Data curation, formal analysis, visualization, methodology, writing–review and editing. **K.S. Bhatia:** Data curation, formal analysis. **C. Wang:** Data curation, formal analysis. **M.S. Pioso:** Data curation, methodology. **X.X. Lin:** Formal analysis. **A.M. Mamdouh:** Data curation, formal analysis. **S.X. Ng:** Formal analysis. **V. Sandhu:** Formal analysis. **S.S. Jasdanwala:** Formal analysis. **B. Yilma:** Formal analysis, methodology. **S. Bohl:** Formal analysis, methodology, writing–review and editing. **J.A. Ryan:** Formal analysis, methodology, writing–review and editing. **D. Malani:** Writing–review and editing. **M.R. Luskin:** Writing–review and editing. **O. Kallioniemi:** Writing–review and editing. **K. Porkka:** Writing–review and editing. **S. Adamia:** Methodology. **W.J. Chng:** Formal analysis. **M. Osato:** Methodology. **D.M. Weinstock:** Methodology, writing–review and editing. **J.S. Garcia:** Methodology, writing–review and editing. **A. Letai:** Conceptualization, resources, supervision, funding acquisition, writing–original draft, project administration. **S. Bhatt:** Conceptualization, resources, supervision, funding acquisition, writing–original draft, project administration.

Acknowledgments

S. Bhatt acknowledges support from the Dana-Farber Cancer Institute Claudia-Adams Barr Award, American Society of Hematology Global Research Award, and the National Medical Research Center of Singapore. S. Bhatt is a recipient of the Leukemia & Lymphoma Society Fellow Award , 2016 AACR Basic Cancer Research Fellowship (Grant Number 16-40-01-BHAT), and EMBO Global Investigator Award. Research reported in this publication was supported by the Ted and Eileen Pasquarello Tissue Bank in Hematologic Malignancies. J.S. Garcia acknowledges support from the NCI of the NIH under award numbers CA066996 and K08CA245209 and the NIH/NCI SPORE in Myeloid Malignancies grant 1P50CA206963. A. Letai and J.S. Garcia acknowledge support from the NIH under award number P01 CA066996. D.M. Weinstock is supported by NCI R35 CA231958 and NCI P50 CA212069630.

Note

Supplementary data for this article are available at Blood Cancer Discovery Online (https://bloodcancerdiscov.aacrjournals.org/).

Received January 1, 2024; revised February 15, 2024; accepted February 19, 2024; published first March 5, 2024.

REFERENCES

1. Bohl SR, Bullinger L, Rücker FG. New targeted agents in acute myeloid leukemia: new hope on the rise. Int J Mol Sci 2019;20:E1983.
2. Short NJ, Konopleva M, Kadia TM, Borthakur G, Ravandi F, DiNardo CD, et al. Advances in the treatment of acute myeloid leukemia: new drugs and new challenges. Cancer Discov 2020;10:506–25.

3. Winer ES, Stone RM. Novel therapy in acute myeloid leukemia (AML): moving toward targeted approaches. Ther Adv Hematol 2019;10: 2040620719860645.
4. Erba HP, Montesinos P, Kim HJ, Patkowska E, Vrhovac R, Zak P, et al. Quizartinib plus chemotherapy in newly diagnosed patients with FLT3-internal-tandem-duplication-positive acute myeloid leukaemia (QuANTUM-First): a randomised, double-blind, placebo-controlled, phase 3 trial. Lancet 2023;401:1571–83.
5. Perl AE, Martinelli G, Cortes JE, Neubauer A, Berman E, Paolini S, et al. Gilteritinib or chemotherapy for relapsed or refractory FLT3-mutated AML. N Engl J Med 2019;381:1728–40.
6. Stone RM, Mandrekar SJ, Sanford BL, Laumann K, Geyer S, Bloomfield CD, et al. Midostaurin plus chemotherapy for acute myeloid leukemia with a FLT3 mutation. N Engl J Med 2017;377: 454–64.
7. DiNardo CD, Jonas BA, Pullarkat V, Thirman MJ, Garcia JS, Wei AH, et al. Azacitidine and venetoclax in previously untreated acute myeloid leukemia. N Engl J Med 2020;383:617–29.
8. Norsworthy KJ, Ko C, Lee JE, Liu J, John CS, Przepiorka D, et al. FDA approval summary: mylotarg for treatment of patients with relapsed or refractory CD33-positive acute myeloid leukemia. Oncologist 2018;23: 1103–8.
9. DiNardo CD, Stein EM, de Botton S, Robox GJ, Atlman JK, Mims AS, et al. Durable remissions with ivosidenib in IDH1-mutated relapsed or refractory AML. N Engl J Med 2018;378:2386–98.
10. Kim ES. Enasidenib: first global approval. Drugs 2017;77:1705–11.
11. Norsworthy KJ, By K, Subramaniam S, Zhuang L, Valle PLD, Przepiorka D, et al. FDA approval summary: glasdegib for newly diagnosed acute myeloid leukemia. Clin Cancer Res 2019;25:6021–5.
12. Stein EM, Aldoss I, DiPersio JF, Stone R, Arellano M, Rosen G, et al. Safety and efficacy of menin inhibition in patients (Pts) with MLL-rearranged and NPM1 mutant acute leukemia: a phase (Ph) 1, first-in-human study of SNDX-5613 (AUGMENT 101). Blood 2021;138(Suppl. 1):699.
13. Hata AN, Niederst MJ, Archibald HL, Gomez-Caraballo M, Siddiqui FM, Mulvey HE, et al. Tumor cells can follow distinct evolutionary paths to become resistant to epidermal growth factor receptor inhibition. Nat Med 2016;22:262–9.
14. Van Allen EM, Wagle N, Sucker A, Treacy DJ, Johanessen CM, Goetz EM, et al. The genetic landscape of clinical resistance to RAF inhibition in metastatic melanoma. Cancer Discov 2014;4:94–109.
15. Yoda S, Lin JJ, Lawrence MS, Burke BJ, Friboulet L, Langenbucher A, et al. Sequential ALK inhibitors can select for lorlatinib-resistant compound ALK mutations in ALK-positive lung cancer. Cancer Discov 2018; 8:714–29.
16. Bell CC, Fennell KA, Chan YC, Rambow F, Yeung MM, Vassiliadis D, et al. Targeting enhancer switching overcomes non-genetic drug resistance in acute myeloid leukaemia. Nat Commun 2019;10:2723.
17. Daver N, Cortes J, Ravandi F, Patel KP, Burger JA, Konopleva M, et al. Secondary mutations as mediators of resistance to targeted therapy in leukemia. Blood 2015;125:3236–45.
18. Fennell KA, Vassiliadis D, Lam EYN, Martelotto LG, Balic JJ, Hollizeck S, et al. Non-genetic determinants of malignant clonal fitness at single-cell resolution. Nature 2022;601:125–31.
19. Marine JC, Dawson SJ, Dawson MA. Non-genetic mechanisms of therapeutic resistance in cancer. Nat Rev Cancer 2020;20:743–56.
20. Bhatt S, Pioso MS, Olesinski EA, Yilma B, Ryan JA, Mashaka T, et al. Reduced mitochondrial apoptotic priming drives resistance to BH3 mimetics in acute myeloid leukemia. Cancer Cell 2020;38: 872–90.
21. Ling Y, Zhang Z, Zhang H, Huang Z. Protein kinase inhibitors as therapeutic drugs in AML: advances and challenges. Curr Pharm Des 2017; 23:4303–10.
22. Maiti A, Franquiz MJ, Ravandi F, Cortes JE, Jabbour EJ, Sasaki K, et al. Venetoclax and BCR-ABL tyrosine kinase inhibitor combinations: outcome in patients with philadelphia chromosome-positive advanced myeloid leukemias. Acta Haematol 2021;143:567–73.
23. Montero J, Sarosiek KA, DeAngelo JD, Maertens O, Ryan J, Ercan D, et al. Drug-induced death signaling strategy rapidly predicts cancer response to chemotherapy. Cell 2015;160:977–89.
24. Pan R, Ryan J, Pan D, Wucherpfennig KW, Letai A. Augmenting NK cell-based immunotherapy by targeting mitochondrial apoptosis. Cell 2022;185:1521–38.
25. Pourzia AL, Olson ML, Bailey SR, Boroughs AC, Aryal A, Ryan J, et al. Quantifying requirements for mitochondrial apoptosis in CAR T killing of cancer cells. Cell Death Dis 2023;14:267.
26. Chonghaile TN, Sarosiek KA, Vo TT, Ryan JA, Tammareddi A, Moore VCG, et al. Pretreatment mitochondrial priming correlates with clinical response to cytotoxic chemotherapy. Science 2011;334:1129–33.
27. Vo TT, Ryan J, Carrasco R, Neuberg D, Rossi DJ, Stone RM, et al. Relative mitochondrial priming of myeloblasts and normal HSCs determines chemotherapeutic success in AML. Cell 2012;151:344–55.
28. Bottomly D, Long N, Schultz AR, Kurtz SE, Tognon CE, Johnson K, et al. Integrative analysis of drug response and clinical outcome in acute myeloid leukemia. Cancer Cell 2022;40:850–64.
29. Malani D, Kumar A, Brück O, Kontro M, Yadav B, Hellesoy M, et al. Implementing a functional precision medicine tumor board for acute myeloid leukemia. Cancer Discov 2022;12:388–401.
30. Tyner JW, Tognon CE, Bottomly D, Welmot B, Kurtz SE, Savage SL, et al. Functional genomic landscape of acute myeloid leukaemia. Nature 2018;562:526–31.
31. Murakami MA, Weinstock DM. Cancer models: the next best thing. Nature 2017;549:39–41.
32. Townsend EC, Murakami MA, Christodoulou A, Christie AL, Koster J, DeSouza TA, et al. The public repository of xenografts enables discovery and randomized phase II-like trials in mice. Cancer Cell 2016;29:574–86.
33. Certo M, Del Gaizo Moore V, Nishino M, Wei G, Korsmeyer S, Armstrong SA, et al. Mitochondria primed by death signals determine cellular addiction to antiapoptotic BCL-2 family members. Cancer Cell 2006;9:351–65.
34. Olesinski EA, Bhatt S. Dynamic BH3 profiling method for rapid identification of active therapy in BH3 mimetics resistant xenograft mouse models. STAR Protoc 2021;2:100461.
35. Horibata S, Gui G, Lack J, DeStefano CB, Gottesman MM, Hourigan CS. Heterogeneity in refractory acute myeloid leukemia. Proc Natl Acad Sci U S A 2019;116:10494–503.
36. Patel C, Stenke L, Varma S, Lingberg ML, Bjorkholm M, Sjoberg J, et al. Multidrug resistance in relapsed AML: Evidence of biological heterogeneity. Cancer 2013;119:3076–83.
37. Zhang J, Gu Y, Chen B. Mechanisms of drug resistance in acute myeloid leukemia. Onco Targets Ther 2019;12:1937–45.
38. Chonghaile TN, Roderick JE, Glenfield C, Ryan J, Sallan SE, Silverman LB, et al. Maturation stage of T-cell acute lymphoblastic leukemia determines BCL-2 versus BCL-XL dependence and sensitivity to ABT-199. Cancer Discov 2014;4:1074–87.
39. Hackl H, Astanina K, Wieser R. Molecular and genetic alterations associated with therapy resistance and relapse of acute myeloid leukemia. J Hematol Oncol 2017;10:51.
40. Hartmann L, Haferlach C, Meggendorfer M, Nadarajah N, Kern W, Haferlaach T, et al. Molecular characterization of acute myeloid leukemia patients who relapse more than 3 years after diagnosis: an exome sequencing study of 31 patients. Haematologica 2020;105:e157–9.
41. Ding L, Ley TJ, Larson DE, Miller CA, Koboldt DC, Welch JS, et al. Clonal evolution in relapsed acute myeloid leukemia revealed by whole genome sequencing. Nature 2012;481:506–10.
42. Gorre ME, Mohammed M, Ellwood K, Hus N, Paquette R, Rao PN, et al. Clinical resistance to STI-571 cancer therapy caused by BCR-ABL gene mutation or amplification. Science 2001;293:876–80.
43. Kobayashi S, Boggon TJ, Dayaram T, Janne PA, Kocher O, Meyerson M, et al. EGFR mutation and resistance of non-small-cell lung cancer to gefitinib. N Engl J Med 2005;352:786–92.
44. Garcia JS, Bhatt S, Fell G, Sperling AS, Burgess M, Keshishian H, et al. Increased mitochondrial apoptotic priming with targeted therapy predicts clinical response to re-induction chemotherapy. Am J Hematol 2020;95:245–50.
45. Olesinski EA, Bhatia KS, Mahesh AN, Rosli S, Mohamed JH, Jen WY, et al. BH3 profiling identifies BCL-2 dependence in adult patients with early T-cell progenitor acute lymphoblastic leukemia. Blood Adv 2023;7:2917–23.

46. Kornauth C, Pemovska T, Vladimer GI, Bayer G, Bergmann M, Eder S, et al. Functional precision medicine provides clinical benefit in advanced aggressive hematologic cancers and identifies exceptional responders. Cancer Discov 2022;12:372–87.
47. Kuusanmäki H, Kytölä S, Vänttinen I, Ruokoranta T, Ranta A, Huuhtanen J, et al. Ex vivo venetoclax sensitivity testing predicts treatment response in acute myeloid leukemia. Haematologica 2022;108:1768–81.
48. Döhner H, Wei AH, Appelbaum FR, Craddock C, DiNardo CD, Dombret H, et al. Diagnosis and management of AML in adults: 2022 recommendations from an international expert panel on behalf of the ELN. Blood 2022;140:1345–77.
49. Khoury JD, Solary E, Abla O, Akkari Y, Alaggio R, Apperley JH, et al. The 5th edition of the World Health Organization classification of haematolymphoid tumours: myeloid and histiocytic/dendritic neoplasms. Leukemia 2022;36:1703–19.
50. Ryan J, Montero J, Rocco J, Letai A. iBH3: simple, fixable BH3 profiling to determine apoptotic priming in primary tissue by flow cytometry. Biol Chem 2016;397:671–8.
51. Nechiporuk T, Kurtz SE, Nikolova O, Liu T, Jones CL, D'Alessandro A, et al. The TP53 apoptotic network is a primary mediator of resistance to BCL2 inhibition in AML cells. Cancer Discov 2019;9:910–25.
52. Dobin A, Davis CA, Schlesinger F, Drenkow J, Zaleski C, Jha S, et al. STAR: ultrafast universal RNA-seq aligner. Bioinformatics 2013;29:15–21.
53. Potdar S, Ianevski A, Mpindi JP, Bychkov D, Fiere C, Ianevski P, et al. Breeze: an integrated quality control and data analysis application for high-throughput drug screening. Bioinformatics 2020;36:3602.